

Topics in Applied Physics – Volume 110

Rainer Behrisch, Wolfgang Eckstein (Eds.)

*Sputtering by Particle Bombardment,
Experiments and Computer Calculations
from Threshold to MeV Energies*

Reprint of the book chapter ”**Chemical Sputtering**”

by W. Jacob and J. Roth published in:
Sputtering by Particle Bombardment, Experiments and Computer
Calculations from Threshold to MeV Energies
R. Behrisch and W. Eckstein (Eds.)
Springer, Berlin 2007, pp. 329 - 400.

The original publication is available at www.springerlink.com

Springer

Berlin Heidelberg New York

Barcelona Budapest Hong Kong

London Milan Paris

Santa Clara Singapore Tokyo

2007

ISBN 987-3-540-44500-5

Contents

Chemical Sputtering

<i>Wolfgang Jacob and Joachim Roth</i>	1
1 Introduction	1
2 Chemical Effects in Sputtering	2
3 Definitions	4
4 Experimental Methods	6
5 Chemical Erosion of Carbon by Atomic Hydrogen	14
6 Chemical Sputtering	20
7 Mechanisms and Modelling for Chemical Sputtering	41
8 Chemical Sputtering with other Reactive Species	57
Index	73

Chemical Sputtering

Wolfgang Jacob and Joachim Roth

Max-Planck-Institut für Plasmaphysik, EURATOM Association, Boltzmannstr. 2,
D-85748 Garching, Germany

Abstract. Chemical effects have to be taken into account if a target is bombarded with chemically reactive species. Two converse effects can occur. Chemical reactions between target and projectile atoms may form species which are more loosely bound to the surface and more easily sputtered. This causes an increase of the sputtering yield. This process is usually subsumed under the expression chemical sputtering. Otherwise, newly formed compounds may possess an enhanced bond strength to the target atoms and, consequently, a higher surface binding energy. This causes a decrease of the sputtering yield compared with the original target.

In this chapter the emphasis is put on sputtering of carbon with hydrogen ions because it is the best studied system. The process of chemical sputtering is defined. The experimental methods to measure it and the available experimental data are discussed. Model conceptions of the basic, microscopic mechanisms developed for chemical sputtering of carbon by hydrogen are reviewed. Finally, several additional species that cause chemical sputtering of carbon materials are presented.

1 Introduction

In 1912, at a time when the basic mechanisms of the erosion of the cathode in a gas discharge were under active discussion, Kohlschütter [1] proposed a process in which volatile radicals are formed in the interaction of the bombarding ions with the target atoms. This model was, however, soon abandoned because cathode erosion was also found in noble gas discharges. In 1926 it was observed [2] that the deposition patterns of sputtered material for some combinations of discharge gas and cathode materials, such as H^+ on C, Bi, Sb, As, and Te were very different from the ones expected and found for non-reactive materials (Fig. 1). For most metals the deposited amount decreases with increasing distance from the cathode as expected. However, for C, Bi, Sb, As, and Te the thickness of the deposits did not decrease, but rather increased with increasing distance from the cathode. This was attributed to the formation of volatile hydrides at the cathode and subsequent cracking by electron impact in the discharge. From this observation Güntherschulze [2] concluded that chemical reactions must have contributed to the erosion. Since then the expression *chemical sputtering* has been used in the literature for the different aspects of the chemical interactions of the projectile and target atoms during sputtering.

About 30 years ago, the chemical aspects of sputtering found renewed interest. In semiconductor technology the strong selectivity of the chemical

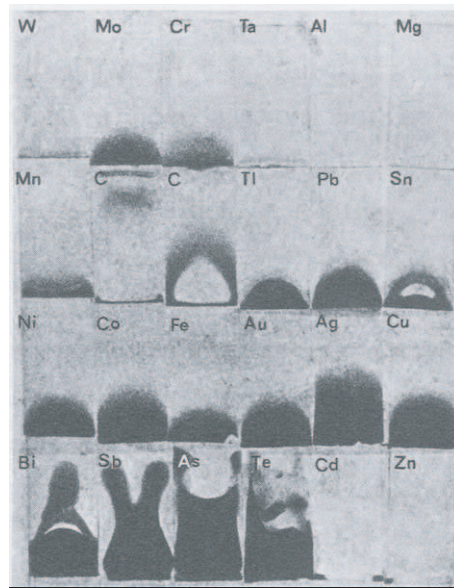


Fig. 1. Deposition of material sputtered from different cathode plates in a hydrogen discharge on a glass plate perpendicular to the cathode surface (from [2])

erosion process depending on the ion–target–atom combination enabled new techniques for etching and structuring of surface patterns [3,4] and for the first time the details of surface reactions leading to volatile molecule formation were investigated for the Si-F system [5].

In fusion research the use of graphite or carbon-fibre composites as plasma-facing material led to large carbon erosion and strong plasma contamination due to the interaction of hydrogen and oxygen ions from the plasma with carbon surfaces [6]. In 1976 the first controlled investigations of carbon erosion due to hydrogen bombardment using ion beams were reported [7–9] and the first atomistic interpretations were proposed [7,8,10]. While in semiconductor technology ion-beam etching has become the basic process for surface structuring [11–13], the improved understanding of the chemical erosion processes of carbon in fusion devices has led to ways of reducing its influence [14–19].

2 Chemical Effects in Sputtering

Energetic ions bombarding a solid are partly backscattered and partly penetrate the surface. They are slowed down and may come to rest near the surface of the material. Bombardment of a solid with ions which react chemically with the atoms of the solid surface may lead to the formation of surface molecules with different binding energies to the surface.

The development of such an altered surface layer has also been found for bombardment by non-reactive ions in a reactive gas atmosphere. If the number of reactive atoms arriving at the surface is comparable or larger than the number of atoms removed by sputtering, a compound layer can be formed which was found to spread over a thickness equivalent to the range of the bombarding ions. This may be formed by recoil implantation and cascade mixing [20–22] or diffusion [23,24] of the atoms implanted in the near-surface layer. The build-up of the altered surface layer generally leads to a different sputtering behaviour than for the original surface. The sputtering yield can be decreased or increased and the composition and the distributions of the sputtered species will be different. Causes of these changes may be divided into two groups:

- Presence of trapped ions: The incident ions may be implanted and chemically bound, forming an altered surface layer. The altered surface layer will modify the spread of the collision cascade, especially if the mass of the trapped ions is very different from the mass of the target atoms, thus decreasing the sputtering yield of the original target atoms [23–31].
- Changes of the binding energies: The compound formed in the surface layer and on the surface will generally lead to formation of molecules with a binding energy to surface atoms which is different from that of the original solid. A lower binding energy will result in an increase of the sputtering yield and a higher binding energy in a decrease of the sputtering yield. For sufficiently low binding energies, thermal desorption of compound molecules can lead to additional erosion. This thermal release will be best observable if the yields from collisional effects are low such as at low bombarding energies.

In addition to their fundamental interest, these effects are of significant importance in a number of technical processes. For example, metal oxides, carbides, and nitrides are produced by reactive sputtering. In reactive sputtering, metal atoms are sputtered from a solid target using typically an argon plasma. A small admixture of an appropriate reactive gas leads to the deposition of the desired layers on the substrate. However, chemical processes occurring at the target surface can also cause an altered surface layer forming a compound that has a higher surface binding energy and thus a lower sputtering yield. This is a major problem for a reliable control of reactive sputtering processes and has recently been discussed by *Sproul* et al. [32]. On the other hand, the enhancement of sputtering yields due to chemical effects, i.e., chemical sputtering, plays an important role in a variety of modern plasma etching [33] processes for fabrication of memory and logic chips in the microelectronics industry [12]. Plasma etching in the semiconductor industry is generally called “dry etching” in contrast to “wet etching” using liquid chemical substances.

Although the involved chemistries for dry etching processes in semiconductor technology and chemical sputtering in the interaction of fusion plas-

mas with carbon-based plasma-facing materials are largely different, the general mechanisms are similar. We will focus in this chapter on the erosion of carbon in the interaction with hydrogen ions because the basic processes in the C-H system as a whole are more comprehensively studied. Since we will touch upon silicon etching only marginally, we refer the interested reader here to some reviews in that field: A survey of phenomena and basic processes occurring in reactive etching in microelectronics, fusion, and space technologies was compiled by *Auciello* and coauthors [34]. The basics of plasma etching are presented in the textbook by *Manos* and *Flamm* [33]. The surface sciences aspects of etching reactions on semiconductor materials have been reviewed by *Winters* and *Coburn* [35].

3 Definitions

Chemical sputtering was investigated in very different fields, such as dry etching of semiconductor materials in microelectronics and erosion of carbon in the thermonuclear fusion community, and by a large number of different groups. As a consequence of this diversity many different names were coined to describe identical processes and different authors have used and still use identical phrases to denote different processes. Actually, many authors have used in the past the phrase chemical erosion synonymously with chemical sputtering. This has led and can still lead to some confusion. In addition, a large number of alternative names has been used for what we call chemical sputtering: chemically enhanced (physical) sputtering [36,37], ion-assisted chemical erosion [38], ion-assisted etching [39], and reactive ion sputtering or reactive ion etching [11–13]. The important phrases with relevance to chemical sputtering which will be used throughout this chapter are defined in this section.

3.1 Physical Sputtering

Physical sputtering is caused by momentum transfer from the impinging projectiles to target atoms. It takes place for all target materials and incident particles with an energy above a threshold energy in the range of about 100 eV. Physical sputtering is reasonably well understood as presented in the Chapter by Eckstein.

Sputtered particles originate predominantly from the topmost surface layer with only small contributions from the second and third atomic layer. In general, they are monoatomic and have mean energies in the eV range, i.e., their kinetic energy is much higher than that of thermally released species.

3.2 Chemical Erosion

Chemical erosion is the process initiated by chemical reactions between neutral, thermal species from the gas phase with surface atoms. For carbon mate-

rials chemical effects are of paramount importance for hydrogen, oxygen, and fluorine projectiles, but chemical effects are also known for other impinging species (e.g. nitrogen).

3.3 Chemical Sputtering

Chemical sputtering is defined as “a process whereby ion bombardment causes or allows a chemical reaction to occur which produces a particle that is weakly bound to the surface and hence easily desorbed into the gas phase” [35]. The erosion process depends on both the kinetic energy and the chemical reactivity of the impinging species. The main effect of ion bombardment is to promote the chemical reaction. The release will mostly be thermally driven.

The occurrence of chemical sputtering may be inferred from a number of different experimental observations.

- Molecules are formed between projectile and target atoms.
- The process varies strongly with the projectile target combination.
- The sputtering yields are significantly higher compared with physical sputtering predictions from computer simulations. In contrast, data for sputtering with noble gases or self-sputtering are, in general, in excellent agreement with such predictions.
- The threshold energy is substantially lower than for physical sputtering.
- The sputtering yield shows a pronounced temperature dependence.
- The energy distribution of the released species should be close to the target surface temperature.

The clearest proof for identification of chemical sputtering is the detection of chemical compounds formed between target and projectile atoms. Newly formed species at the surface can have a lower surface binding energy and are consequently more easily sputtered such that the sputtering yield increases. This is a possible indication for chemical sputtering and, in fact, it was frequently used in the literature [25]. On the other hand, newly formed compounds can have a higher surface binding energy than the corresponding unreacted surfaces and, as a consequence, the sputtering yield decreases. This is, for example, the case for oxygen, carbon, or nitrogen bombardment of various metals where metal oxides (Al_2O_3 , SiO_2 , TiO_2 , etc.), carbides (TiC, WC, SiC, etc.), and nitrides (TiN) are formed.

Physical sputtering shows a negligible temperature dependence if the temperature is well below the melting point of the material [40–42]. For carbon, however, a strong increase of the sputtering yield close to the sublimation temperature was reported for all bombarding ions. This process was named radiation-enhanced sublimation (RES) [43–46]. In contrast, chemical sputtering shows a strong temperature dependence significantly below melting or sublimation temperatures. This has been observed in systems where chemical interactions between target and projectile atoms play a significant role. A

prominent, but not unique, example which has been thoroughly investigated is the interaction of hydrogen with carbon. Such a temperature dependence can in principle be caused by activation of chemical reactions and/or by activation of diffusion of species produced in deeper layers.

A significant deviation of the energy distribution of released species from that of physically sputtered particles is also an indication of chemical sputtering. While physically sputtered species have mean energies of a few eV, chemically sputtered species which are released by a thermal desorption process after a chemical reaction at the surface have an energy distribution which is determined by the surface temperature. In the case of hydrogen ions impinging on carbon surfaces at a temperature of 800 K the dominant fraction of released molecules has a thermal energy distribution corresponding to the surface temperature [47]. On the other hand, for bombardment at room temperature the emitted CH_3 radicals have a significant suprathermal component which is, however, also different from a distribution of species produced by physical sputtering [47].

A further indication of chemical sputtering can be deduced from the re-deposition pattern. Indeed, the first experimental observation of chemical sputtering by *Güntherschulze* [2] (see Fig. 1) was based on the observation of differences in the deposition pattern. Physical sputtering leads to deposition almost exclusively at surfaces which are in line of sight of the particle source. However, chemically released radical species, which can survive several wall collisions can also be transported to remote areas which are not in line of sight. A method to investigate this effect is presented in Sect. 4.5.

A new sputtering mechanism named: 'Swift Chemical Sputtering' was discovered in molecular dynamics simulations [48–53]. Swift chemical sputtering leads to the release of hydrocarbon radicals (including single C atoms) down to energies of about 2 eV by a kinetic emission process. The 'Swift Chemical Sputtering' process has recently been shown to occur also for bombardment with helium ions [54]. It is a new process which differs from usual physical sputtering and from chemical sputtering.

4 Experimental Methods

To achieve a relatively complete picture of the underlying physical and chemical processes, two or more experimental methods have to be combined. In laboratory experiments, the most frequently applied methods to determine the total erosion yields are weight loss measurement, ellipsometry, and mass spectrometry. The latter is also applied for identification of released species. In plasma experiments, optical emission spectroscopy of different excited hydrocarbon fragments is employed to determine chemical sputtering yields.

4.1 Weight Loss

The total erosion yield can be obtained from the weight loss of the sample after bombardment with a certain ion fluence. Weight loss measurements can be performed using vacuum micro-balances with sensitivities of the order of $1 \mu\text{g}$ [55,56] or quartz oscillators, where the frequency shift due to the mass loss of a deposited layer is determined (see, e.g., Refs. [57–59]). By proper calibration sensitivities of the order of sub-monolayers can be achieved using quartz microbalances [57–59]. Quartz microbalance measurements require preparation of thin film systems while vacuum balance measurements can be applied to bulk samples. Weight loss measurements have the advantage to integrate over all possible mass loss processes and all types of species. In contrast to mass spectrometry, different sensitivities for different eroded molecules do not play a role. The main disadvantage of the weight loss method arises in cases where the incident particles accumulate in the target and give rise to uncontrolled weight increases [60]. For hydrogen on carbon, as for most metals, the amount of retained hydrogen can be neglected compared with the weight loss due to erosion provided the ion fluence is sufficiently high [61]. The need to accumulate high fluences until measurable weight changes are obtained, makes the method unsuited for investigating fluence dependences of the erosion yield [62]. Consequently, weight loss measurements determine in general the steady-state value of the sputtering yield. The precision of the measured yields increases with increasing total weight change. Therefore, at sufficiently long measuring times, weight loss measurements in steady state produce the most precise sputtering yields.

4.2 Mass Spectrometry

Identification of released species using a remote mass spectrometer in the sputtering chamber is a very useful method to verify chemical sputtering. However, the species measured in the remote mass spectrometer may also be formed on other wall areas by reflected projectiles. Indeed, extensive production of CH_4 on the walls of the sputtering chamber by atomic hydrogen reflected from the substrate led to a higher CH_4 signal than the reaction at the sample surface and thus hampered these early attempts to measure the interaction of atomic hydrogen with carbon surfaces [63–65]. But the wall may act not only as particle source but also as sink. Reactive species or long chain hydrocarbons which may be produced in the interaction with the sample may stick to the chamber walls [66] or be converted to other species. In any case, if a remote mass spectrometer is used, species reach the ionizer only after many wall collisions and, in general, only stable or so-called recycling species contribute to the signal. Thus, in practise, a remote mass spectrometer merely measures the partial pressure of stable molecules that builds up in the vacuum chamber. In general, it cannot measure species with a high sticking probability.

A big advantage of mass spectrometry is that it produces real-time data and allows measuring parameter variations in much shorter times than weight loss measurements. However, the determination of total chemical sputtering yields by mass spectrometry requires extensive data evaluation and interpretation. Firstly, the sensitivity of the mass spectrometer has to be properly calibrated for each eroded species. For many species this can be achieved by appropriate calibration procedures with stable gases [67,68], but for reactive species, such as hydrocarbon radicals, this method fails. Secondly, if the eroded particle flux comprises more than one species and their cracking patterns produced by the ionisation process in the ion source of the mass spectrometer overlap, then the measured mass spectra have to be decomposed into the individual contributions. In most cases the cracking pattern cannot be determined for all species in the mixture, and the inverse problem is therefore ill posed. Routines used for the decomposition of multi-component mass spectra like the recursive method [69] or least square fits [70] provide only poor and sometimes nonphysical results such as negative concentrations [69]. Recently, advanced analysis techniques were developed using Bayesian probability theory [71,72] and a generalized maximum entropy approach [73].

A frequently used method for quantifying mass spectrometry data is measuring the intensity of a certain mass signal and relating this to the flux of a released species. In simple cases in particular, if the number of produced species is small, such a signal can be attributed to one species only and by comparison to other methods, e.g., to weight loss data, it can possibly be quantified. But this works reliably only in few favorable cases. What can be measured in this case is the production rate of one or a few released species. Whether or not this production rate is proportional to the total sputtering yield has to be thoroughly checked. Unfortunately, the erosion of carbon materials by hydrogen suffers from several problems: Firstly, depending on experimental conditions, the product spectrum of released species can be very rich [74–79]. Secondly, the product spectrum of released species changes as a function of experimental parameters. E.g., for the chemical sputtering of metal-doped carbon materials it was shown that the methane yield increases with dopant concentration while the total yield decreases strongly [19]. Under such conditions the quantification of total sputtering yields is very challenging. Due to the mentioned inherent problems in the quantification of mass spectrometric data for the chemical sputtering of carbon by hydrogen, there has always been a systematic disagreement with weight loss data [80,81]. Weight loss resulted in most cases in higher chemical sputtering yields than mass spectrometric investigations. The disagreement decreased with the consideration of higher hydrocarbons, but it did not vanish completely.

A possibility to circumvent or reduce the contribution of species produced at the chamber walls to the measured signal is using a line-of-sight mass spectrometry setup. But even if the mass spectrometer has a line of sight to the surface of interest, the signal is in most cases dominated by recycling

species. This shall be explained by the following sample calculation. Let us assume that we have a flow of stable species leaving the surface. The ionizer of the mass spectrometer is in line of sight with the sample in a direction perpendicular to the sample surface and has a distance x from the surface. Species that go directly to the ionizer of the mass spectrometer contribute to the beam component of the signal, species that go to other chamber wall areas are reflected and contribute to the background pressure in the chamber. The mass spectrometer signal is determined by the particle density in the ionizer of the mass spectrometer. As a consequence, the beam-to-background ratio of the mass spectrometer signal, R_{bb} , is given by the ratio of the particle densities due to the directed beam, n_{beam} , and the background density, $n_{background}$ [82]. The background pressure and therewith the background density are determined by the effective pumping speed, S_{eff} , of the pumping system. If we neglect all other possible background contributions R_{bb} is given by [82]

$$R_{bb} = \frac{n_{beam}}{n_{background}} = \frac{S_{eff}}{\pi x^2 \bar{v}_{beam}} . \quad (1)$$

Here \bar{v}_{beam} is the average velocity of the beam particles. The denominator πx^2 accounts for the reduction in the flux density for a cosine distribution in a distance x [83]. Equation (1) demonstrates that the beam-to-background ratio depends critically on two parameters: the effective pumping speed, S_{eff} , of the chamber and the distance of the ionizer of the mass spectrometer from the particles' origin. A typical value for the effective pumping speed of a vacuum system is 100 l/s. Let us for simplicity assume that the distance is 10 cm (in real cases the distance is often larger). If we then assume that the species is a methane molecule and leaves the sample surface with a mean velocity according to a room temperature distribution, we can calculate R_{bb} . This yields a value of about 5×10^{-3} (for CH_4). It is obvious that under such conditions it is virtually impossible to discriminate beam particles from background. Even if the distance x is reduced to 1 cm, which is practically impossible, R_{bb} increases only to 0.5. The preceding estimate is still rather optimistic because all other contributions to the background signal are neglected. In addition, R_{bb} will further decrease if the particles leave the surface with a temperature higher than 300 K or if they are even emitted with some kinetic energy, such as, for example, in physical sputtering where the sputtered particles have energies in the eV range.

The preceding discussion has shown that a line-of-sight setup is necessary but not sufficient to detect reactive species and that significant effort has to be spent to reduce the signal contribution of recycling species. This can be achieved by putting the mass spectrometer in a separate vacuum chamber which is differentially pumped. Such a measurement geometry is often named molecular beam mass spectrometry (MBMS). Furthermore, for quantification of the species fluxes it is not sufficient to reduce the contribution from the isotropic background, but in addition its magnitude has to be determined.

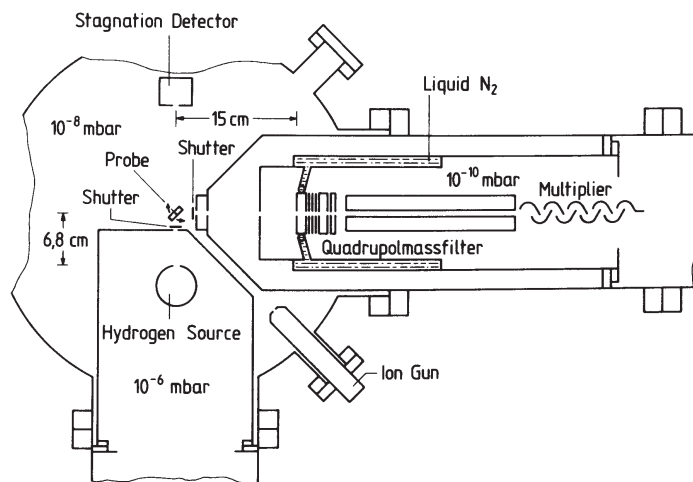


Fig. 2. Experimental setup of Vietzke et al. [77,85]

This can be done with a simple flag or with a continuous chopper connected with lock-in data acquisition. The flag or chopper has to be placed directly in front of the ionizer in the last pumping stage. If the flag or chopper is situated in one of the differential pumping stages, or even in the sample chamber, care has to be taken to account for the modulation of the background in the ionizer. The direct background measurement is then only possible when the chopping period is shorter than the residence time of the species [84].

Vietzke and colleagues used a line-of-sight setup such that any reaction product or sputtered species is detected directly without hitting a wall [77,85]. The experimental setup of Vietzke et al. is shown in Fig. 2. Surface-scattered species and reaction products are detected in a two-stage differentially pumped quadrupole mass spectrometer positioned perpendicular to the hydrogen-beam direction. The housing around the QMS and part of its ionizer is cooled by liquid nitrogen to reduce background signals in the QMS chamber. Background signals from the main chamber are subtracted from the measured signal by chopping the particle flux inside the reaction chamber. However, this chopping in the reaction chamber can cause a modulation of the background signal and thus hamper a correct analysis. The sensitivity of the QMS is determined by a Knudsen cell placed at the position of the target. This setup is able to detect about 10^{10} product molecules per second.

4.3 Ellipsometry

Ellipsometry is an optical method that measures the change of polarization upon reflection from a surface. It is applicable to thin transparent films on

a reflecting surface. Where it is applicable, it has significant advantages over other methods. Its biggest advantage is its very high sensitivity, which allows detection of changes at the surface of less than a monolayer.

The physical quantities that can be extracted from ellipsometry measurements are the complex refractive index of a thin film and its thickness. Since ellipsometry measures only the thickness change during an experiment, the density of the material has to be known from other measurements to convert the thickness change into the number of sputtered atoms. Details of ellipsometry can be found in the textbook of *Azzam and Bashara* [86]. Its application to the investigation of thin carbon layers is described in Refs. [38] and [87].

Owing to its very high sensitivity, only a few monolayers of material have to be removed to get reliable results. Thus, it is orders of magnitude faster than weight loss measurements and transient changes in the sputtering yield can be followed. Moreover, ellipsometry is sensitive to changes of the optical properties of thin overlayers which may be caused by ion bombardment [38,87–90]. This enables very detailed studies of the interaction of ions with surfaces. Among other effects ellipsometry is sensitive to surface roughness.

4.4 Optical Emission Spectroscopy

In a plasma environment, species released from the surface can be detected by optical emission spectroscopy (OES). Hydrocarbon molecules and radicals formed at the surface by chemical erosion or chemical sputtering penetrate the edge plasma after being released from the surface. By collisions with plasma electrons they may become ionized, dissociated, or excited. The released amount of carbon can be quantified from the analysis of the radiation emitted from these molecular species. However, this requires a rather detailed modelling of the hydrocarbon dissociation chain and knowledge about the excitation mechanisms of the individual species and of their possible sticking to surfaces. Many studies in very different experimental environments such as edge plasmas of tokamak devices [91–103], plasma generators (PISCES [104], PSI-1 [105]), and laboratory plasmas [106–109] have been performed.

The determination of particle fluxes from spectroscopy measurements in a plasma was thoroughly discussed by *Behringer et al.* [110] for the case of atom and ion fluxes. The analysis for molecular species is in principle very similar, but in addition to the ionization, the dissociation of the molecules has to be modelled, which adds further uncertainties. Important spectroscopic quantities that have to be determined from calibration measurements and/or theoretical models are the S/XB and D/XB ratios ("inverse photon efficiencies" for ionisation and dissociation, respectively) that link measured photon fluxes of break-up products to the corresponding particle fluxes [110,111]. The related problems were discussed by *Brezinsek et al.* [112]. For the time being, these spectroscopic quantities which depend on the actual plasma conditions are a matter of ongoing discussion [93,95,104,112,113]. As a consequence,

OES data are relatively simple to measure, but hard to quantify and relate to the initially sputtered species. In that sense, they are similar to the problems encountered in mass spectrometry. An advantage of OES is that it delivers real-time data and allows online measurements in a plasma environment such as in the boundary layers of fusion devices where particle fluxes are very high. Measurements at these high, fusion-relevant fluxes are only possible with OES.

4.5 Cavity Probes

A further method for investigating properties of released species is determining the redeposition pattern. In general, physical sputtering produces species with some kinetic energy which have a high sticking probability. As a consequence, these species can only be deposited in line of sight from their place of origin. On the other hand, chemical sputtering produces thermal species with largely varying sticking probabilities. Such species can survive many wall collisions and therefore be transported also to areas which have no direct line of sight to the sputtered surface. These two different sputtering processes lead to very different redeposition patterns [2].

The effective surface loss probability of released species can be determined by measuring the deposition pattern in a well-defined geometry, e.g., using cavity probes [114–120]. This method has recently been applied to investigate the redeposition of species produced during chemical sputtering of graphite with hydrogen ions [66]. Clearly, the determination of surface loss probabilities with cavity probes does not allow determining the species spectrum, but it is a relatively simple, qualitative method to discriminate between physical and chemical sputtering.

4.6 Dedicated Multiple Beam Experiments

Most experiments for chemical sputtering have been carried out using a single ion beam. But a number of different groups investigated chemical sputtering processes applying dedicated multiple beam setups using, e.g., an atom beam and an ion beam. A big advantage of multiple beam setups compared with single beam setups is that they can provide a much better insight into the underlying microscopic processes and phenomena.

Vietzke and coworkers investigated the simultaneous interaction of beams of atomic hydrogen and argon ions using a molecular beam mass spectrometer (MBMS) setup [47,77,121] which was briefly described in Sect. 4.2. It allows the independent control of atomic hydrogen flux and ion flux and an identification of the released species. Due to the MBMS configuration not only stable molecules, but also radical species can be measured and quantified. A later upgrade to a time-of-flight mass spectrometer [47] also enabled the determination of the energy distribution of the released species.

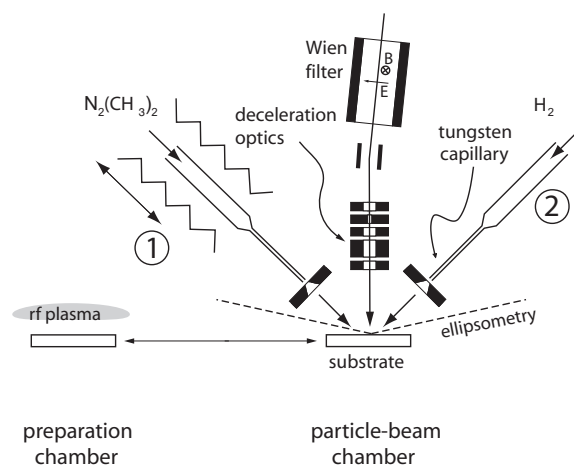


Fig. 3. Sketch of the MAJESTIX setup. The main components in the particle-beam chamber are the ion gun system, two radical beam sources, and a line of sight for the in-situ ellipsometry diagnostic. Each radical source can either be run with H_2 or D_2 to produce atomic H and D, respectively

Dual beam experiments were also carried out at the university of Toronto. This dual beam accelerator experiment [122] comprises two independent ion beam sources and was applied to study a variety of simultaneous irradiation phenomena with two different ion beams. They studied the simultaneous irradiation of graphite with C^+ and H^+ ions [123], noble gas ions (He^+ , Ne^+ , Ar^+) and H^+ ions [122,124,125], D^+ and H^+ ions [126–128], O^+ and H^+ ions [129–133], and tungsten erosion due to low energy O^+ and D^+ impact [134]. For detection of released species they used a remote mass spectrometer.

Winters and Coburn studied the etching of silicon due to irradiation with fluorine and argon ions [35]. Etch products, recombination products or reflected incident species were detected by the modulated-beam line-of-sight mass spectrometric detection system. There are four stages of differential pumping between the sample and the mass spectrometer. A mechanical chopper inside the reaction chamber modulates the flux of surface-scattered species and reaction products. Sample surface conditions are periodically monitored by an Auger electron spectrometer.

A variety of particle-beam experiments were performed in the MAJESTIX device at IPP Garching [135–142]. A sketch of the experimental setup is shown

in Fig. 3. MAJESTIX is an UHV-based particle-beam experiment comprising two radical beam sources and one source for low energy ions [143]. As a diagnostic tool, real-time in-situ ellipsometry is implemented. The fluxes of the radical beam sources are absolutely quantified for production of hydrogen atoms and methyl radicals [144,145]. The ion source can produce a wide variety of ionic species, e.g. He^+ , Ne^+ , Ar^+ , H^+ , H_2^+ , H_3^+ , N_2^+ , and CH_3^+ . Ion energies from above 1 keV down to 1 eV are achievable. The setup allows to investigate heterogeneous surface processes of one single species or the simultaneous interaction of up to three different, individually-controllable species with a surface of interest. Running one of the radical sources to produce atomic hydrogen and the ion source with the mentioned ions, microscopic surface processes such as chemical sputtering, can be studied in great detail.

5 Chemical Erosion of Carbon by Atomic Hydrogen

5.1 Thermal Process

Chemical erosion of carbon by hydrogen is a thermally activated process which does not require energetic species. Chemical erosion of graphite due to thermal atomic hydrogen has been studied in great detail using a variety of diagnostics for the surface hydrogen content, the hybridisation of carbon atoms in the surface layer, and the emitted species [10,16,63–65,74–78,85,146–158].

The first quantitative investigations originate from 1975 from modulated atomic-hydrogen-beam experiments by *Balooch* and *Olander* [10]. Atomic hydrogen was produced in an oven at a temperature of 2000 K and impinged onto pyrolytic graphite samples. The reaction probability was measured by determining the intensity of emitted hydrocarbons in a quadrupole mass spectrometer as a function of the surface temperature. Below about 800 K, CH_4 was the dominant reaction product, whereas C_2H_2 evolved at temperatures above 1200 K. The results were explained by a detailed atomistic model assuming an atomic hydrogen gas in thermal and chemical equilibrium with the solid surface. However, agreement with the data could only be obtained assuming that atomic hydrogen and methane molecules only partly reach equilibrium at the carbon surface, the equilibration probability decreasing strongly with increasing temperature.

Around 1995 the individual steps in the erosion process have been elucidated and quantitatively described by cross sections and activation energies [155]. The atomistic steps of the chemical reaction of thermal atomic hydrogen with a thin amorphous hydrogenated carbon layer (a-C:H) on platinum were investigated in detail for atom fluxes of about $10^{17} \text{ m}^{-2}\text{s}^{-1}$ [151,155,156]. The hybridisation stages of the involved carbon atoms from graphitic sp^2 to hydrogenated sp^3 were analysed using high resolution electron energy loss spectroscopy (HREELS), while the hydrogen and hydrocarbon content of the layer were determined by thermal desorption spectroscopy (TDS). Together

H-atom induced chemical erosion

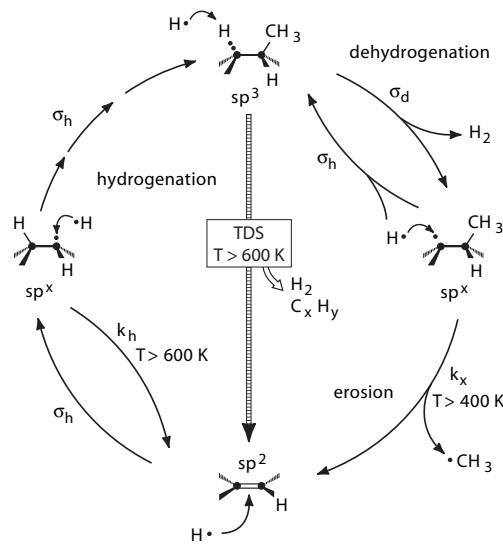


Fig. 4. Chemical erosion cycle of graphite in the interaction with thermal atomic hydrogen [155,157]

with isotope exchange experiments between hydrogen and deuterium, this resulted in a description of the reaction scheme by four individual processes shown schematically in Fig. 4 and summarised here:

Even at low temperatures sp^2 carbon atoms at the edges of graphitic planes or with broken bonds are hydrogenised to sp^3 hydrocarbon complexes via an intermediate radical stage sp^x (left-hand side of Fig. 4). The hydrogenation is not thermally activated, but proportional to a cross section σ_h for the subsequent addition of hydrogen. Further irradiation with thermal atomic hydrogen will also lead to hydrogen molecule formation and desorption with a cross section, σ_d , leaving a radical stage sp^x with a broken bond in the a-C:H network (right-side of Fig. 4). Due to the much larger value of σ_h compared with σ_d the sp^x concentration will only be about 2-4% of the sp^3 concentration.

With increasing temperature, different thermally activated processes will become possible: at temperatures around 400 K chemical erosion can occur. Hydrocarbon complexes attached to the a-C:H network in the neighbourhood of sp^x radicals (right-side of Fig. 4) can be desorbed with a rate constant k_x by simultaneously joining the neighbouring free bond to a double bond, thus returning to the basic graphitic sp^2 configuration. On a fully hydrogenated surface the last step of radical sp^x formation is rate limiting for erosion. With further increasing temperature, however, incoming hydrogen atoms may recombine with adsorbed atoms above 600 K with a rate constant k_h (left-hand

side of Fig. 4), thus interrupting the hydrogenation process and, therefore, reducing the sp^3 concentration and subsequent chemical erosion. Thus, the erosion rate will exhibit a maximum at intermediate temperatures. For the given experimental parameters [151,155,156] this maximum occurs around 600 K. If the hydrogen irradiation is stopped, already available hydrocarbon complexes can be desorbed above 600 K (indicated by the central arrow in Fig. 4).

For each hybridisation state of carbon, i.e. sp^2 , sp^x and sp^3 a balance equation can be formulated in steady state. The equations can be solved for the concentration of sp^3 complexes [155,159].

$$c^{sp^3} = \frac{\sigma_h \Phi + k_x}{\sigma_h \Phi + \left(1 + \frac{\sigma_d k_h}{\sigma_h^2 \Phi}\right) k_x}, \quad (2)$$

$$k_x = A \cdot \exp(-E_{therm}/kT), \quad (3)$$

$$k_h = B \cdot \exp(-E_{rel}/kT). \quad (4)$$

k_x and k_h are the thermally activated rate coefficients, as described above, with the activation energies E_{therm} and E_{rel} and the pre-exponential factors A and B . All necessary model parameters, i.e., σ_h , σ_d , k_x , k_h , A , and B were quantitatively determined from experiments [151,155,156].

In contrast to earlier assumptions made by *Erents* et al. [8] and *Busharov* et al. [9] the erosion yield related to an incident atomic hydrogen flux Φ is not dependent on the hydrogen concentration but on the concentration of hydrogenated sp^x centres. In steady state the erosion rate is given by the product of c^{sp^x} with k_x and n_0 , n_0 being the total number density of carbon surface sites per unit area (for graphite, $n_0 = 2.3 \times 10^{19} \text{ m}^{-2}$). c^{sp^x} is given by

$$c^{sp^x} = c^{sp^3} \frac{\sigma_d \Phi}{\sigma_h \Phi + k_x}. \quad (5)$$

The corresponding erosion yield Y_{therm} is given by the erosion rate divided by the flux

$$Y_{therm} = \frac{n_0 c^{sp^x} k_x}{\Phi} = \frac{n_0 c^{sp^3} k_x}{\Phi} \frac{\sigma_d \Phi}{\sigma_h \Phi + k_x} = \frac{n_0 \sigma_d k_x}{\sigma_h \Phi + \left(1 + \frac{\sigma_d k_h}{\sigma_h^2 \Phi}\right) k_x}. \quad (6)$$

The model parameters are given in table 1. The resulting erosion yield is shown in Fig. 5 as a function of temperature, together with the erosion data for thermal atomic hydrogen [155]. At room temperature chemical erosion is negligible, and above 600 K the erosion decreases due to the recombinative release of hydrogen molecules. The maximum yield at 600 K is about 9×10^{-3} C atoms per H atom.

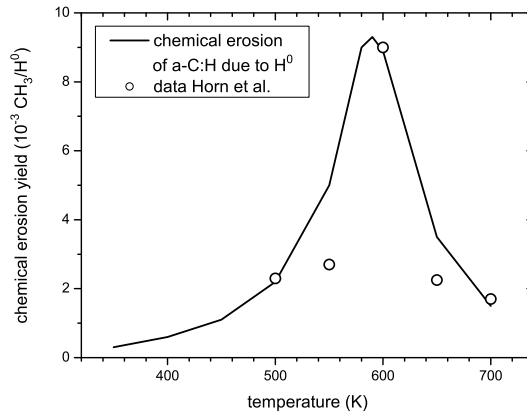


Fig. 5. Model results for chemical erosion of amorphous hydrocarbon layers due to interaction with thermal atomic hydrogen (atom flux about $10^{17} \text{ m}^{-2}\text{s}^{-1}$) [155]. The circles show experimental data from *Horn et al.* [155]

The reaction of atomic hydrogen with different grades of graphite [160] was also investigated. It was found that the scatter of the data between different samples of the same grade of up to a factor of 2 is of similar magnitude as the scatter between different graphites. From this fact, they concluded that there is no significant influence of the type of graphite on the reaction of atomic hydrogen. On the other hand, experiments by *Vietzke et al.* have shown that the reactivity of graphite towards atomic hydrogen is greatly enhanced—by more than one order of magnitude—if the surface is irradiated by energetic ions prior to the experiment [77,79]. It was concluded that the chemical attack of hydrogen on graphite requires active surface sites (dangling bonds) which are in this experiment produced by the preceding ion bombardment. This is in accordance with the conclusions made by *Küppers* and coworkers [157] who have shown that undisturbed graphitic planes are essentially unreactive towards atomic hydrogen. Hydrogen can react only with the edges of graphitic planes. Ion bombardment of well-ordered graphitic regions produces plenty of additional reaction centres. This causes a significant increase of the reaction yield. The deposition of impurities (e.g., nickel [160]) significantly reduces the reactivity at the surface.

Table 1. Model parameters for calculating the chemical erosion yield according to (6) [155]

σ_d (m^2)	σ_h (m^2)	A (s^{-1})	B (s^{-1})	E_{therm} (eV)	E_{rel} (eV)
0.05×10^{-20}	4.5×10^{-20}	1×10^{13}	1×10^{13}	1.61	1.73

5.2 Species Released by Chemical Erosion

According to the reaction scheme elaborated by Küppers and coworkers, the primary erosion product of the thermally driven chemical erosion process is CH_3 [157]. This was indeed measured by *Vietzke* and coworkers [85] who have shown that in the reaction of atomic hydrogen with graphite CH_3 dominates over CH_4 (Fig. 6). The maximum yield in their experiments was found to be around 500 K. No significant influence of the type of graphite on the reaction of atomic hydrogen with graphite has been found [77,160]. The reaction probability is below 10^{-4} , i.e., it is much lower than the yield determined by *Horn* et al. [155] (see Fig. 5). *Horn* et al. investigated carbon layers with a thickness of only a few monolayers deposited on a Pt substrate. For this model system all carbon atoms can be assumed to be available for hydrogen attachment and the model agrees reasonably well with the experimental data without a free fit parameter. For the application to chemical erosion of graphitic materials the only available sites for hydrogen bonding and chemical erosion are edge atoms of graphitic planes or damage sites due to ion bombardment [157]. To account for that, an additional scaling parameter C was introduced which defines the height of the peak maximum [80]. A comparison of Figs. 5 and 6 suggests that this scaling parameter has to be of the order of 10^{-2} for chemical erosion of graphite. A further improvement of (6) first suggested by *Horn* et al. [155] and later introduced by *Roth* [80] was: instead of using a fixed value for the activation energy E_{therm} for CH_3 release, a Gaussian distribution of activation energies with a standard deviation of 0.3 eV was used.

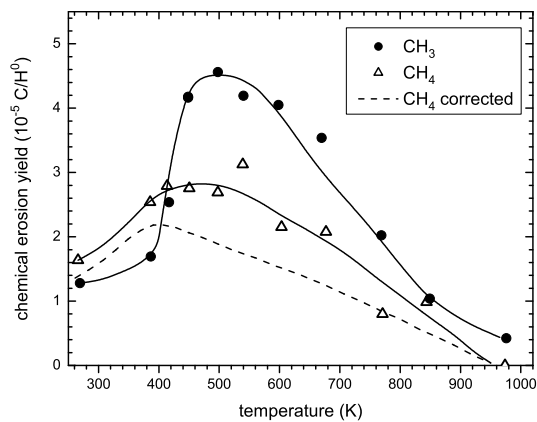


Fig. 6. Temperature dependence of the production yield of CH_3 and CH_4 for chemical erosion of graphite with thermal atomic hydrogen ($1.6 \times 10^{20} \text{ m}^{-2} \text{ s}^{-1}$) [85]. The dashed line (CH_4 corrected) is obtained by correcting the measured CH_4 signal with the CH_4 signal originating from recombination of CH_3 at the chamber walls

This broadens the chemical erosion peak and leads to a better agreement with experimental data.

In addition to CH_3 and CH_4 formation, C_2H_y species were also detected [77]. Quantitative studies by *Davis et al.* [161], who used a remote mass spectrometer to measure stable species, have shown that the chemical erosion by thermal hydrogen atoms is clearly dominated by C_2 and C_3 hydrocarbons. The production of CH_4 accounts for only 5-10% of the total erosion yield.

In addition to graphite, the erosion of amorphous hydrogenated carbon (a-C:H) films by thermal atomic hydrogen was investigated by *Vietzke et al.* [78,148,162]. a-C:H layers are a model system for a graphite surface being irradiated by hydrogen ions (this point will be discussed in more detail in Sect. 6.1). The main reaction product is the radical CH_3 . It is accompanied by a wide variety of other hydrocarbons including other radicals. CH_3 , C_2H_y , and C_3H_y species are formed with a relative proportion of 1:0.8:0.5. The temperature maxima for the different products occur at different temperatures. The maximum for CH_3 production is at 750 K, that for C_2H_y at 650 K, and that for C_3H_y at 520 K. The total chemical erosion yield as well as the product spectrum depend strongly on the a-C:H structure. The yield is much higher than for graphite. The total chemical erosion yield at 520 K for hard a-C:H films is about 0.014 and for soft, polymer-like films it increases to 0.05 and even to 0.16 depending on the actual film structure. In contrast, the yield for graphite is of the order of 10^{-4} . The reaction of deuterium with hard a-C:H films leads predominantly to fully deuterated hydrocarbon species. The hydrogen from the layers is released as HD. This means that the isotope exchange with the layer is much faster than the chemical erosion process. This finding is again in excellent agreement with the reaction scheme proposed by *Küppers et al.* which was discussed in Sect. 5.1.

The product distribution of chemical erosion of thin, hard a-C:H layers was studied in detail by *Zecho et al.* [74,75]. If a thin a-C:H film is exposed to a flux of atomic hydrogen (a flux of about $10^{20} \text{ H m}^{-2}\text{s}^{-1}$ was used in these experiments), C_1 and C_2 hydrocarbons are the main products, but contributions of higher hydrocarbons (C_3 to C_8) were detected as minority species. C_1 and C_2 hydrocarbons exhibit an erosion maximum around 750 K, while C_3 to C_5 hydrocarbons show a maximum around 650 K. The quantitative analysis of the data demonstrates that the hydrogen-induced chemical erosion of a-C:H films is dominated by formation of C_2 hydrocarbons (see Fig. 7). About 50% of the eroded carbon atoms appear in this channel. The maximum erosion yield at around 750 K is 0.1 C/H. The product distribution found by *Zecho et al.* is in good agreement with the earlier work of *Davis et al.* [161] who investigated graphite instead of a-C:H layers. But the absolute yields are, as earlier found by *Vietzke et al.* [78,148,162], much higher for a-C:H compared with graphite. Although the yield of *Zecho et al.* is in accordance with that of *Vietzke et al.*, the product distributions differ somewhat. This can be attributed to a difference in the structure of the a-C:H layers inves-

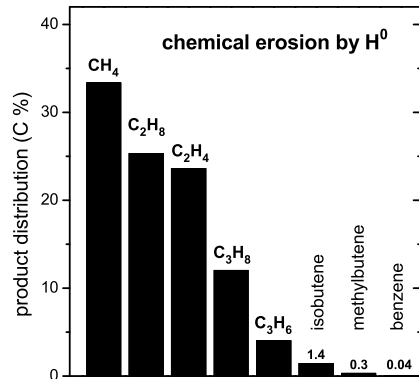


Fig. 7. Product distribution of the H-atom-induced chemical erosion of a thin, hard amorphous hydrocarbon layer (16 nm thick) from a temperature programmed erosion experiment in the temperature range 300 to 1000 K (heating rate 0.5 K/s) [74]. Shown is the fraction of the total number of carbon atoms eroded via the respective channel [74]

tigated by both groups. It was shown by *Vietzke et al.* [78,148,162] that the film structure has a great influence on the total yield, so it can be assumed that it also influences the product distribution.

Zecho et al. [75] also investigated the influence of thermally induced structural changes of a-C:H films on the chemical erosion. Annealing of the films at 1100 K leads to a partial regraphitization, but hydrogen atoms rapidly rehydrogenate the surface even at temperatures of up to 800 K. Consequently, this annealing does not change the erosion yield; however, it influences the product distribution and the temperature dependence. The erosion of annealed a-C:H films is dominated by formation of C₂ hydrocarbons followed by C₁ and C₃ species; C₄ and C₅ occur as minority species.

6 Chemical Sputtering

As defined in Sect. 3 we subsume under the phrase chemical sputtering all processes where the erosion process depends on both the kinetic energy and the chemical reactivity of the impinging species. In experiments this can appear in two different cases: i) bombardment with reactive ions (e.g., H⁺) where the ion carries the kinetic energy and is chemically reactive and ii) combined bombardment by noble gas ions and reactive thermal species where the energy is supplied by the noble gas ion and the chemically active species has only thermal energy. These two different cases are discussed in the two following subsections. In addition, more complicated cases are possible if instead of noble gas ions reactive ions are used (e.g., H₂⁺ and atomic H). In chemical sputtering experiments all three basic erosion mechanisms—chemical erosion,

physical sputtering, and chemical sputtering—may be active. To what extent they influence the measured effects depends on the experimental parameters, particularly on the energy of the ions and the temperature of the sample.

An early review of chemical sputtering in general was compiled by J. Roth in a chapter in a preceding volume of this series [36]. Over the years, several review articles summarized the status of knowledge of the interaction of hydrogen atoms and ions with carbon surfaces. Auciello et al. reviewed the synergism in materials erosion due to multispecies impact in 1985 [163]. The erosion of graphite due to particle impact was reviewed by *Roth*, *Vietzke*, and *Haasz* in 1991 [164] and later on by *Vietzke* and *Haasz* in 1996 [16]. In that period most of the experiments in this field were motivated by thermonuclear fusion research. The fuel for a fusion plasma are hydrogen isotopes and large areas of the plasma-facing components are made of carbon materials so that the interaction of energetic and atomic hydrogen species with carbon surfaces is a very important plasma-surface-interaction process. The majority of these experiments was carried out using beams of hydrogen ions at energies between several ten eV up to some keV.

6.1 Chemical Sputtering with Reactive Ions

The chemical sputtering of graphite by hydrogen ions is a complex process depending on surface temperature, ion flux, surface state of the material, and energy of the incident particles. Although these various experimental parameters show strong interdependences, we discuss them in the following separate subsections.

6.1.1 Temperature Dependence

Initially discovered by *Günterschulze* [2] in 1926, chemical sputtering of carbon due to bombardment by hydrogen ions found renewed interest in 1976. The first systematic investigations of chemical sputtering were carried out simultaneously by several groups (*Roth* et al. [7], *Erents* et al. [8,165], and *Busharov* et al. [9]). All of these early experiments studied the temperature dependence of the CH₄ production rate during bombardment of different carbon grades with hydrogen ions using a remote mass spectrometer. Ion energies in the range from 100 eV up to 30 keV were used.

The results are summarized in Fig. 8. The common observation of all these experiments is that the CH₄ production yield increases with increasing target temperature, reaches a maximum in the range of about 900 K, and decreases for further increasing temperature. In this view, already the first experiments proved two mandatory requirements for a chemical sputtering process: i) the erosion process produces molecules comprising target and projectile atoms and ii) the process shows a pronounced temperature dependence. Soon thereafter, *Yamada* et al. 1980 [166] published similar results with a maximum yield at $T_{max} = 800$ K. We will see later that this temperature value depends

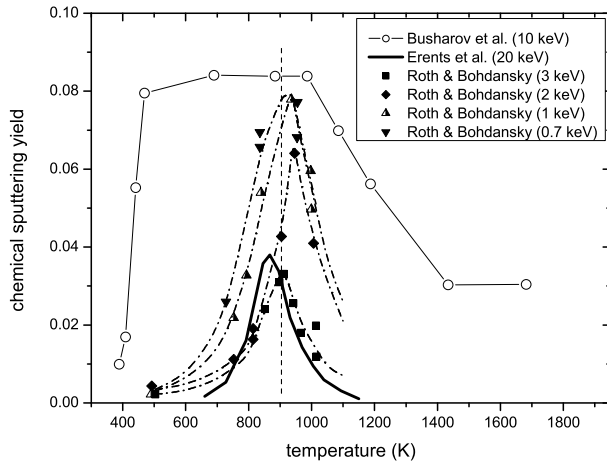


Fig. 8. Compilation of the early results from 1976 by Roth et al. [7], Erents et al. [8,165], and Busharov et al. [9] showing the temperature dependence of chemical sputtering of graphite due to bombardment with hydrogen ions at different energies. Note that the value and position of the maximum depend on ion flux and energy

on the ion flux. Following investigations corroborated these early findings and extended the experimental data base [76,79,85,148,167–169]. This early work has been reviewed by Roth et al. [164] in 1991 and by Vietzke and Haasz [16] in 1996.

The occurrence of a maximum yield for chemical sputtering with energetic hydrogen ions at the temperature T_{max} was assumed to result from the competition of an exponential increase of the reaction rate between carbon and hydrogen with an even stronger decrease of the hydrogen concentration in the surface at temperatures exceeding 800 K. At lower temperatures the lattice concentration of hydrogen saturates and the reaction rate increases with increasing temperature, while at higher temperatures the recombinative hydrogen release decreases the hydrogen content so that the reaction rate decreases [8,9].

Details of the temperature dependence and the value of the maximum erosion yield depend on ion flux and energy as will be discussed in the following subsections.

6.1.2 Energy Dependence

Already the first published results about chemical sputtering of carbon by hydrogen isotopes as presented in Fig. 8 [7,8] have shown that the maximum chemical sputtering yield depends strongly on the ion energy. In the following years, different aspects of the energy dependence were studied in great detail [44,81,159,166,169–180]. However, in the initial publications, only the

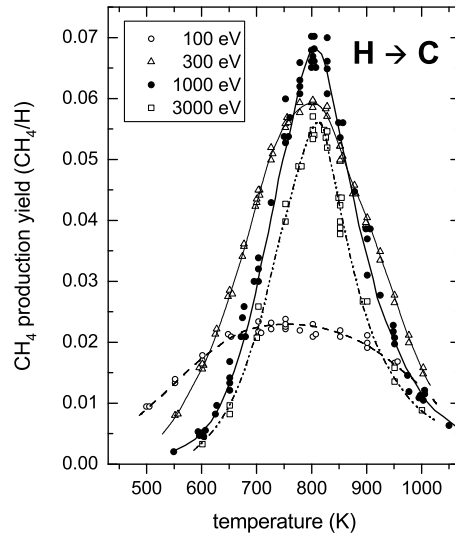


Fig. 9. Methane production yield as a function of substrate temperature for hydrogen ions with different energies impinging on pyrolytic graphite [170]. H_3^+ ions with three times the indicated energy have been used in this experiment. The ion flux density was $\approx 1 \times 10^{20} \text{ m}^{-2}\text{s}^{-1}$ and beam at normal incidence. The production yield is, as in all comparable following figures, normalized to the number of hydrogen atoms in the used molecular ion

methane production yield was determined and it was implicitly assumed that this is equivalent to the total chemical sputtering yield. This assumption is, however, not valid, as will be further discussed in Sect. 6.1.5.

Over the years, the energy and temperature dependence of the methane production yield due to high energy ($> 300 \text{ eV}$) hydrogen ion bombardment of graphite have been investigated by several groups producing relatively consistent results [7–9,44,148,160,165,166,170,173]. A typical set of methane production yields as a function of temperature for different ion energies is shown in Fig. 9 [170]. In this experiment pyrolytic graphite samples were bombarded with H_3^+ ions of different energies. The methane production was measured by residual gas analysis using a remote mass spectrometer. Between ion energies of 300 and 3000 eV (per H^+ , i.e., 900 to 9000 eV per H_3^+ ion) methane production peaks at a temperature of 800 K ($T_{max} = 800 \text{ K}$). At lower ion energy (100 eV/ H^+) the peak broadens and the maximum shifts to slightly lower temperatures such that below about 600 K the methane production yield is even higher than for bombardment with high energy ions. The energy dependence of the data from Fig. 9 is presented in Fig. 10. The maximum yield peaks at about 600 eV per H^+ with a value of about 0.085

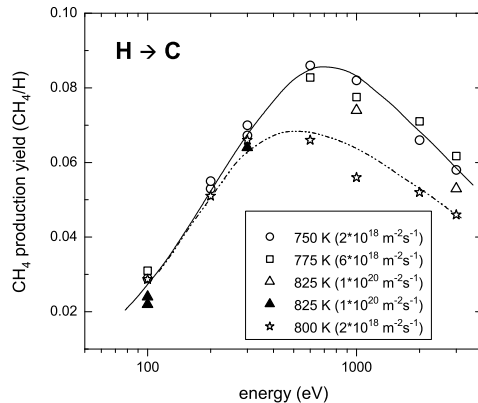


Fig. 10. Methane production yield as a function of ion energy for hydrogen ions impinging on pyrolytic graphite [170]. The *solid line* shows the yields determined from data similar to those presented in Fig. 9 at the individual temperature maximum for each energy value. The *dashed line* shows the corresponding yield determined for a fixed temperature of 800 K. Different symbols correspond to different applied ion fluxes. The experimental parameters (target temperature and ion flux) are given in the legend

CH_4/H (flux = $2 \times 10^{18} \text{ m}^{-2}\text{s}^{-1}$) [170]. We note that the yield shows a slight flux dependence (Sect. 6.1.4).

Yamada et al. measured the methane production yields of various types of carbon in the energy range from 100 to 6000 eV [166]. The curves have a distinct maximum around 1 keV (see Fig. 11). For higher energies the yield decreases. This general behaviour is the same for all investigated temperatures ranging from 620 to 870 K. They found the highest yield of about 0.07 methane molecules per impinging H^+ ion for an energy of 1 keV ($T_{max} = 800 \text{ K}$). Roth et al. have shown in total weight loss measurements that the maximum of the energy dependence shifts to lower energy with decreasing temperature. The maximum measured at 300 K is at about 300 eV [44], while measurements at T_{max} result in an energy of maximum yield of about 1 keV in agreement with Yamada et al. [166]. Because the shape of the energy dependence was found to be strikingly similar to physical sputtering, the influence of similar knock-on effects was assumed to be responsible. Mech et al. [175,176] extended the energy range down to 10 eV and indeed found a decrease of the maximum chemical sputtering yield indicating a threshold at energies around a few eV.

Experimental results for the sputtering of carbon by hydrogen and deuterium ions determined by weight loss measurements are shown in Fig. 12 for sample temperatures of 300 K and T_{max} . The solid line in Fig. 12 shows the result of the 'Eckstein-Preuss fit formula' (see Chapter by Eckstein) which is based on TRIM.SP calculations and provides a good quantitative description

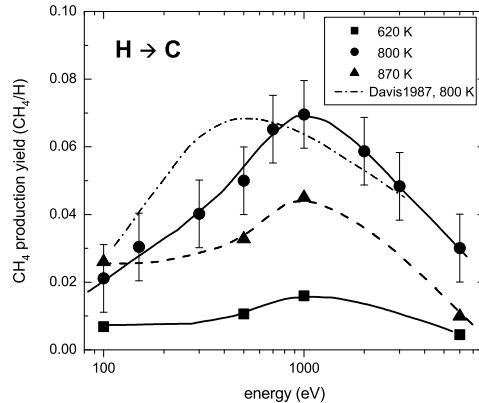


Fig. 11. Methane production yield as a function of ion energy for hydrogen ions impinging on pyrolytic graphite measured at different sample temperatures [166]. The ion flux density was $\approx (3 \text{ to } 12) \times 10^{18} \text{ m}^{-2}\text{s}^{-1}$ and beam at normal incidence. For comparison, the data from Fig. 10 (measured at 800 K and $2 \times 10^{18} \text{ m}^{-2}\text{s}^{-1}$) are also shown

of physical sputtering. At sample temperatures of 300 K and ion energies exceeding ~ 200 eV the observed rates are in reasonable agreement with the theoretical data (Fig. 12) and can thus to a large extent be explained by physical sputtering. However, the experimental values in this range are consistently higher than the results of the analytic description. *Küstner et al.* [181] have shown that this difference is partially due to the roughness of the real graphite surface. On the other hand, chemical sputtering may still contribute to the total erosion in this energy range, so it is not surprising that the measured data lie above the theoretical data for pure physical sputtering.

At energies below 100 eV the measured yields do not decrease as anticipated for physical sputtering when approaching the threshold energy, but they remain constant [81,159]. It was even found that the yield remains constant down to temperatures of about 100 K [18,182]. A prominent isotope effect is observed with yields for deuterium being higher by a factor of 5 to 7. For higher energies (> 100 eV) the isotope effect is only a factor of 2 to 3. The energy dependence at T_{max} shows higher yields than at 300 K, the increase being more pronounced at energies above 100 eV. In this energy range increased damage formation enhances the chemical reactivity throughout the implantation range.

6.1.3 Dependence on the Type of Graphite

Chemical sputtering of carbon by hydrogen ions shows a significant dependence of the initial sputtering yield on the type or grade of graphite used for the experiment [166]. With increasing ion fluence strong transient effects

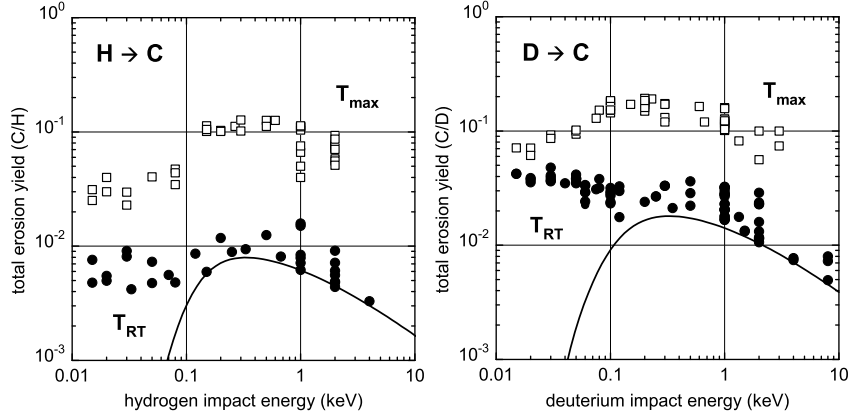


Fig. 12. Energy dependence of the erosion yield of a variety of different carbon materials due to bombardment with H^+ and D^+ ions at room temperature and at T_{max} for the respective energy ($T_{max} = 570 - 920$ K) [81]. The *solid line* shows the result of the 'Eckstein-Preuss fit formula' which describes physical sputtering (see also Fig. 8 in Chapter by Eckstein)

occur, but the energy and temperature dependences of the steady-state yields are not affected by the structure of the different types of carbon. This was attributed to the amorphisation of the sample surface due to the ion bombardment. The dependence of the yield on structural properties is particularly high at very low energy or for reaction with atomic hydrogen [183], where no amorphisation occurs. In general, steady-state yields were obtained after the target was bombarded with proton fluences of more than $1 \times 10^{22} H^+ m^{-2}$ [160,166,169]. The methane production yield for amorphous hydrogenated carbon (a-C:H) layers is, in general, significantly higher than for graphite [78,148,162,168].

The fact that the steady-state yields of chemical sputtering of graphite due to hydrogen ion bombardment are relatively insensitive to the type of graphite is explained by the following: If graphite is bombarded with energetic hydrogen isotopes (ions), the unreflected fraction of the isotopes is implanted into the graphite and initially retained to 100% [76,184–193]. Concomitantly, radiation damage is produced within this range. With increasing ion fluence, the local concentration of hydrogen increases and an increasing fraction of the implanted hydrogen is reemitted. The saturation concentration of hydrogen in carbon at 300 K is about 30% ($H/C \approx 0.4$) ([167,186,187,189]) and it decreases with increasing temperature. When the local concentration exceeds the saturation limit, 100% of the locally implanted hydrogen are reemitted [194] mainly in form of H_2 molecules [190,192,193], but also in form of hydrocarbons [85,125–127,195]. These hydrogen and hydrocarbon molecules are formed at the end of the ion range [85,125–127,190,192,195]. With further in-

creasing fluence, the saturated region increases until it reaches the surface. Then steady state is reached and the whole implantation range is saturated with hydrogen. Any further implanted hydrogen ion is reemitted. The fluence required to reach this saturation is naturally dependent on the ion energy and substrate temperature. For typical energies used for the investigation of chemical sputtering, i.e., in the low keV range, this saturation fluence at room temperature is in the 10^{21} m^{-2} to 10^{22} m^{-2} range [166,76]. After such a fluence, an altered amorphous layer with a significant hydrogen content has developed at the graphite surface [196–198]. The material that is formed at the surface is comparable to "hard" a-C:H layers produced by plasma deposition from methane low-pressure gas discharges as, e.g., in laboratory studies [38,199] or during carbonisation of fusion devices [6,200]. While considerable variation exists in the structural characteristics of these films, mostly depending on ion energies and impinging species fluxes during deposition [38], the hydrogen content of "hard" a-C:H layers is similar to that of hydrogen implanted graphite, i.e., $\text{H/C} \approx 0.4$ at 300 K. Within this altered surface layer the different properties of different types of graphite have disappeared.

6.1.4 Flux Dependence

The position of the temperature maximum of the chemical sputtering yield increases with increasing ion flux [44,159]. At fluxes above $10^{21} \text{ m}^{-2} \text{ s}^{-1}$ as reached in plasma-wall interaction in nuclear fusion experiments, the temperature maximum, T_{max} , reaches values of about 1000 K. At these elevated temperatures, the thermodynamic equilibrium of the H/C system shifts from CH_4 formation to H_2 release [201] and the erosion yield is expected to decrease with ion flux. Additionally, the onset of graphitisation will lead to the annealing of radiation damage resulting in the suppression of reactivity of the carbon material. The coupling of the flux dependence with the temperature dependence leads to conditions where emission of hydrogen molecules prevents the chemical erosion. This has led to the prediction that at such high fluxes the yield at T_{max} decreases.

Efforts to determine a flux dependence in ion beam experiments [170,202] in the flux range of $10^{19} - 10^{20} \text{ D}^+ \text{ m}^{-2} \text{ s}^{-1}$ did not yield conclusive results within the scatter of the data. Actually, measuring the erosion yield at fixed temperature, rather than at T_{max} , resulted in slowly increasing yields at low fluxes and decreasing yields at higher fluxes, as T_{max} passed across the temperature of the measurements [170]. The first indication for a decrease of the yield at high ion fluxes came from measurements on hydrocarbon production at the limiter in the DITE tokamak [203] where hardly any CH A–X band intensity, indicative for methane production, could be detected spectroscopically above the background. Later, the use of plasma simulators and edge plasmas in tokamaks has widely increased the data basis and measured chemical erosion yield data are available from the plasma simulators PSI-1

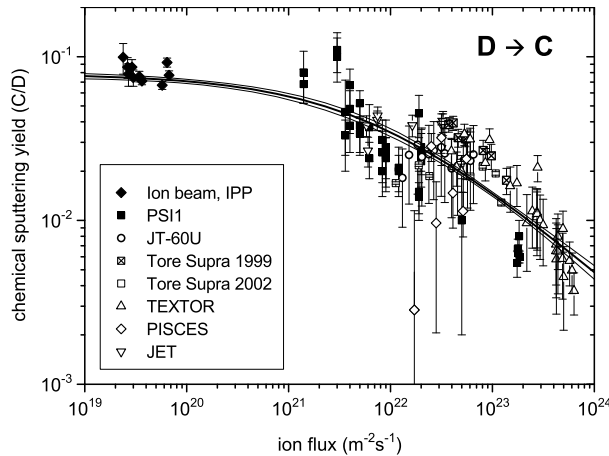


Fig. 13. Flux dependence of the chemical sputtering yield for deuterium at T_{max} and an ion energy of 30 eV determined from ion beam experiments and spectroscopic measurements in different fusion devices and plasma simulators [210]. The *solid lines* are a fit using Bayesian probability theory and its confidence intervals [211]. The experimental data are from the following sources: ion beam experiments (IPP) [81], linear plasma devices PSI-1 [105,204] and PISCES B [104], plasma edge and divertor measurements in the fusion experiments JET [93], Tore Supra [205,206], TEXTOR [207], and JT-60 U [209]

in Berlin [105,204], PISCES B in San Diego [104], and from plasma edge and divertor measurements in fusion facilities, such as JET [93], Tore Supra [205,206], TEXTOR [207], ASDEX Upgrade [102,208], and JT-60 U [209]. However, until 1998 [80] the flux dependence at high fluxes could not be clarified within the scatter of the available data due to the differing conditions of ion energy and surface temperature.

In 2004, an attempt was made to normalise all data to the same conditions, such as particle energy and surface temperature [210]. From ion beams and plasma simulators most of the data were obtained at 30 eV, and all data from tokamaks were subsequently normalised to these conditions using the known dependences on ion energy and substrate temperature.

After this re-evaluation and normalisation of the data, a consistent set of high flux data for methane production at T_{max} is available (see Fig. 13). The data are for deuterium ions, normalised to an incident ion energy of 30 eV and taken at or near T_{max} . While individual data sets in a narrow range of fluxes cannot distinguish clearly flux dependences, the ensemble of data points suggests a decrease of the erosion yield with ion flux starting at fluxes of about $10^{21} \text{ m}^{-2}\text{s}^{-1}$. The model for the functional dependence was

$$Y(E, T, \Phi) = Y_{low}(E, T) / (1 + (\Phi/\Phi_0)^z) \quad (7)$$

where $Y_{low}(E, T) = 0.08$ is given by low flux data from ion beams, Φ_0 is the flux where the transition to a flux dependence occurs, and z is the power of the decrease at high fluxes. Bayesian probability theory was employed to determine the free parameters of the model function [212]. The resulting fit indicates a decrease of the yield at high fluxes with $z = 0.54$ and $\Phi_0 = 6 \times 10^{21} \text{ m}^{-2}\text{s}^{-1}$ [211]. The thin solid lines in the figure give the confidence interval of the resulting fit, predicting a yield of $(5 \pm 0.5) \times 10^{-3}$ at a flux of $10^{24} \text{ m}^{-2}\text{s}^{-1}$, in contrast to previous conservative estimates of 3×10^{-2} [80].

The flux dependence, as given in (7) for the erosion yield at T_{max} seems also to apply at room temperature as obtained from data measured in the fusion experiment ASDEX Upgrade [102]. Therefore, it can be assumed that at all temperatures the same flux dependence occurs.

6.1.5 Identification of Species Released by Chemical Sputtering

While the first investigations of chemical sputtering concentrated on the detection of CH_4 molecules, later work also included measurement of higher hydrocarbons (C_xH_y , $x \geq 2$) [161,169,172,175,176,183,213].

Investigating the contributions of higher hydrocarbon species (C_xH_y , $x \geq 2$) to the chemical sputtering of graphite [172,213] an unexpected finding was

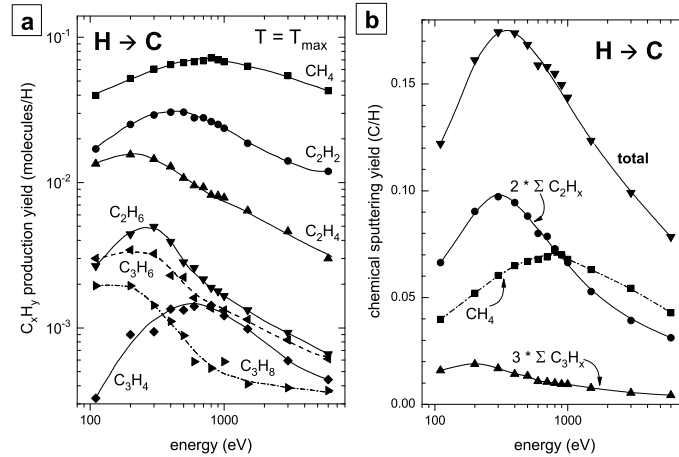


Fig. 14. a) Production yields for C_1 , C_2 , and C_3 hydrocarbons as a function of ion energy measured at the individual, energy-dependent maximum temperature T_{max} [172]. b) chemical sputtering yields, calculated from the data in a) by multiplying the production yields with the number of carbon atoms in the corresponding hydrocarbon species. The contributions of C_1 , C_2 , and C_3 hydrocarbons are shown separately together with the total yield calculated from the sum of these three components

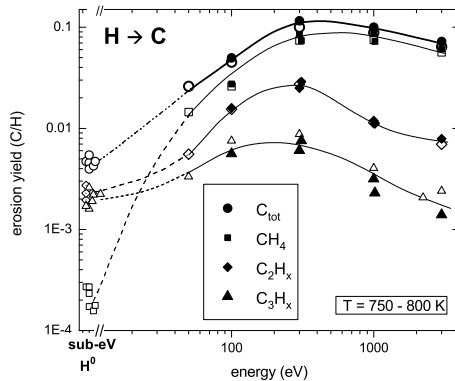


Fig. 15. Production yields for C_1 , C_2 , and C_3 hydrocarbons as a function of ion energy measured at $T = 750$ to 800 K [169]. In addition to ion beam data also erosion yields for thermal H^0 (sub-eV H^0) are shown. Lines are only a guide to the eye. Open and closed symbols belong to different experimental campaigns

made: The product spectrum changes dramatically with ion energy. In addition, the temperature maxima for different species behave differently for different ion energies, so that a sound determination of the total sputtering yield by mass spectrometric methods becomes a rather laborious task. Bombarding a graphite surface with hydrogen ions between 0.1 and 6 keV the maximum of the CH_4 production was found around 750 K. The corresponding maxima for C_2 and C_3 species are shifted to somewhat lower temperatures. The shifts are larger for higher hydrocarbons and for lower energies. For example, the peak for C_3H_6 at 400 eV ion energy is at about 650 K.

The hydrocarbon production yields as a function of ion energy are displayed in Fig. 14. For energies higher than about 1 keV the chemical sputtering yield is still dominated by CH_4 production. However, at energies below about 1 keV the contribution of C_2 species to the total erosion yield dominates. The contribution of C_3 species remains small in the whole energy range, although the relative contribution increases strongly with decreasing energy. Fig. 14b clearly demonstrates that the maximum of the total carbon erosion yield at about 350 eV differs significantly from the maximum of CH_4 production at about 800 eV.

Experiments by Davis et al. [161,169] yielded very similar results with the exception of the contributions of C_2 hydrocarbons (Fig. 15). The C_2 production yields of Davis et al. are in general a factor of $3-4$ lower than those of Yamada [172] (Fig. 14). The reason for this discrepancy was attributed to a fluence dependence of C_2 hydrocarbon formation [214], but remains unresolved quantitatively. As a consequence, the total chemical sputtering yield is in the experiments by Davis et al. in the whole investigated energy range (50 to 3000 eV) dominated by CH_4 production. The relative contribution of

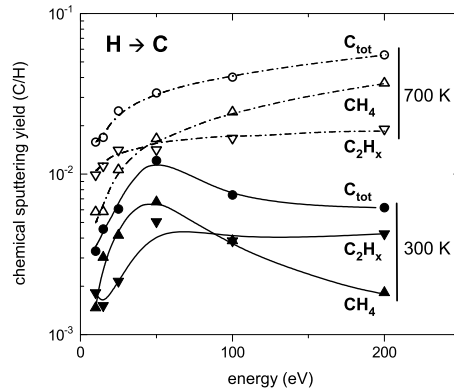


Fig. 16. Energy dependence and product distribution of chemical sputtering of graphite due to bombardment with hydrogen ions measured at $T = 350$ and 700 K [176]

C_2 and C_3 species increases, as in Yamada's experiments, with decreasing ion energy, but remains below 50% in all cases. An extrapolation of ion beam results to thermal energies [169] suggests that the contribution of C_2 and C_3 species should dominate at energies below about 30 eV (Fig. 15). In later experiments at very low energies it was indeed found to dominate at energies below about 50 eV [175,176] (Fig. 16).

Due to the fact that the hydrocarbon product spectrum changes as a function of ion energy and substrate temperature, the total chemical sputtering yield shows a different behaviour than the methane production yield (see Figs. 14 to 16). This can even lead to the fact that the methane production stays constant or increases at low ion energies while the total chemical sputtering yield, which is dominated by heavier hydrocarbons, decreases [18,19,182].

One point that has to be addressed here is a critical comparison of mass spectrometry and weight loss measurements. There has always been a significant difference between chemical sputtering yields determined by mass spectrometry and those determined by weight loss measurements. For the first investigations, this was due to the fact that only methane production yields have been measured by mass spectrometry. The discussion in this section has clearly shown that methane is not the only hydrocarbon species produced. In a certain parameter range, the chemical sputtering yield may be dominated by methane production, but in many cases the yield is dominated by the sum of the contributions of higher hydrocarbons (see Figs. 7, 14, 15, and 16). The consideration of the contributions of C_1 , C_2 , and C_3 hydrocarbon has significantly reduced the difference between the yields measured by mass spectrometry and weight loss, but still a systematic difference remains. It has been shown that this is not due to experimental uncertainties if

comparing results from different experiments, but this difference occurs also for measurements in the same experiment [80,81]. The reason is, that some of the species released by chemical sputtering are highly reactive and stick to the chamber walls [66,81]. As a consequence, total chemical sputtering yields and correct particle flux distributions for the interaction of hydrogen with carbon surfaces can only be measured by molecular-beam mass spectrometry (see Sect. 4.2). A remote mass spectrometer or a simple line-of-sight setup is not sufficient for that purpose. What can be reliably measured by mass spectrometry are production yields of stable molecules which are not lost or transformed at the chamber walls.

6.2 Combined Irradiation with Noble Gas Ions and Hydrogen Atoms

Chemical sputtering has also been investigated with two independent particle beams, namely thermal hydrogen atoms and argon ions [77,85]. The fundamental advantage of this approach is that the chemical and physical interactions of the species with the surface can be controlled independently. In these experiments, a graphite target was exposed to a flux of thermal hydrogen atoms ($1.6 \times 10^{20} \text{ m}^{-2}\text{s}^{-1}$). An additional simultaneous flux of 5 keV argon ions ($1.1 \times 10^{17} \text{ m}^{-2}\text{s}^{-1}$) caused a synergistic enhancement of the hydrocarbon production yield from about $6 \times 10^{-5} \text{ C/H}^0$, measured for atomic hydrogen irradiation alone (Fig. 6), to about $6 \times 10^{-3} \text{ C/H}^0$ (Fig. 17). The enhancement factor depends on the type of ion, the ion energy, and the H-atom-to-ion flux ratio. The temperature dependence is very similar to the

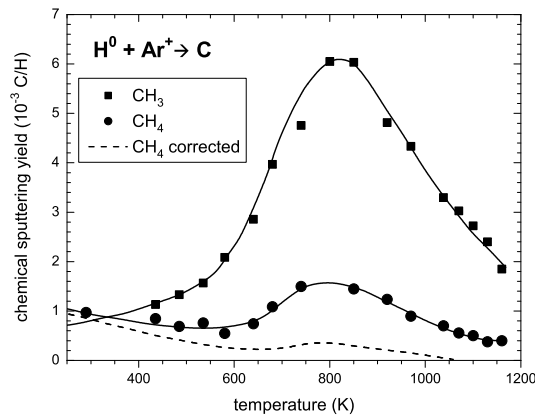


Fig. 17. Temperature dependence of the production yield of CH_3 and CH_4 for chemical sputtering of graphite due to combined irradiation with thermal atomic hydrogen ($1.6 \times 10^{20} \text{ m}^{-2}\text{s}^{-1}$) and argon ions ($1.1 \times 10^{17} \text{ m}^{-2}\text{s}^{-1}$, 5 keV) [85]. The *dashed line* (CH_4 corrected) is obtained by correcting the measured CH_4 signal with the CH_4 signal originating from recombination of CH_3 at the chamber walls

case of bombardment with hydrogen ions only and shows a maximum of the yield at 800 K. On the other hand, no enhancement was found when using molecular hydrogen instead of atomic hydrogen. Obviously, a new mechanism was active that requires the simultaneous interaction of energetic ions and atomic hydrogen. This mechanism is chemical sputtering as defined in Sect. 3. It is important to mention that *Vietzke et al.* determined the sputtering yield by mass spectrometry using an MBMS setup (see Sect. 4.2). Therefore, they were also able to detect radical species. They found that CH_3 is the dominantly released species under these experimental conditions, but CH_4 and higher hydrocarbons are also produced [77,85].

An important finding of this seminal work by *Vietzke et al.* was that their results were not in agreement with the earlier model by *Erents et al.* [8]. As a consequence, this model had to be discarded. *Vietzke et al.* concluded that the collisional energy transfer from the energetic ions to the carbon lattice must be responsible for the drastic enhancement of the yield. A substantial contribution of electronic excitation was excluded due to the results of co-bombardment of graphite with energetic electrons and atomic hydrogen, which did not show a significant enhancement of the sputtering yield [63,64,77]. The basic explanation for the strong synergistic effect is a competition between annealing of defects which are produced by the ions and reaction of atomic hydrogen with these defects. Later *Vietzke* and coworkers also investigated chemical erosion due to exposure to thermal atomic hydrogen of carbon pre-irradiated by different ion species [79]. They found that the erosion yield exceeds that of atomic hydrogen alone by more than one order of magnitude and that the amount of hydrogen bonded in the surface is less important than the damage produced during the ion bombardment. This supports the earlier assumption of the importance of nuclear damage due to the ion bombardment.

Different aspects of chemical sputtering by co-bombardment with ions and hydrogen atoms were investigated using a variety of different ion species. Haasz and coworkers investigated chemical sputtering of graphite using hydrogen [161,215,216] and carbon ions [37]. Initially they focused their work on the determination of the methane production rate by mass spectrometry [215,216]. Later they also measured the production rate of larger hydrocarbons (Fig. 18) [161]. The synergistic methane yield shows a distinct temperature dependence similar to irradiation by hydrogen atoms only. The methane production yield increases with increasing temperature, shows a maximum between 750 and 800 K [161,215,216], and then decreases again. With decreasing ion energy, a noticeable broadening of the peak shape occurs [216]. The methane production yield depends on the ion energy and the atom-to-ion flux ratio [161,215]. As for the ions-only case, the product spectrum changes with ion energy. The relative contribution of higher hydrocarbons increases significantly with decreasing ion energy and varies also with the atom-to-ion flux ratio [161]. In contrast to the ions-only case, where methane is the dom-

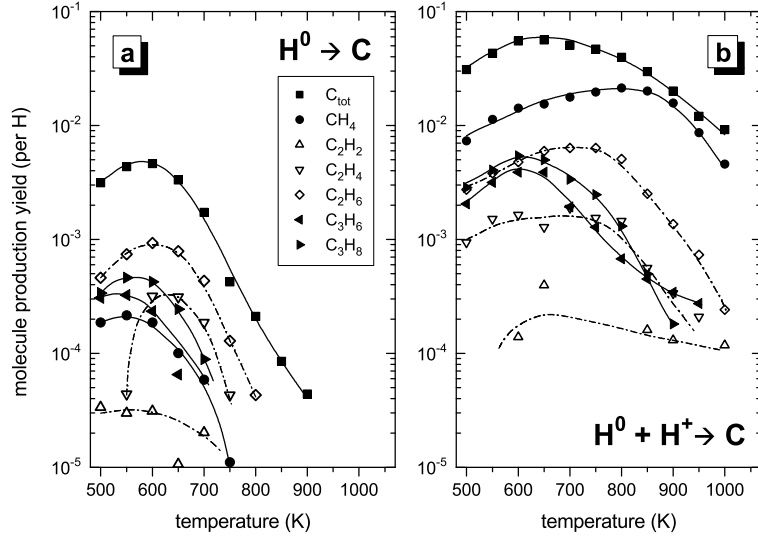


Fig. 18. Molecule production yields and total erosion yields as a function of temperature for bombardment of graphite with (a) atomic hydrogen alone ($1.1 \times 10^{19} \text{ m}^{-2}\text{s}^{-1}$) and (b) combined with hydrogen ions (H^0 : $1.8 \times 10^{19} \text{ m}^{-2}\text{s}^{-1}$; H^+ (900 eV H_3^+): $2.1 \times 10^{18} \text{ H}^+ \text{ m}^{-2}\text{s}^{-1}$) [161]

inant product in most of the energy range, the synergistic erosion due to ion and hydrogen atom co-bombardment is dominated by the sum of higher hydrocarbons (C_2 and C_3) in the whole energy range (50 eV to 3 keV) [161] (Fig. 18b). Due to the contribution of higher hydrocarbons, the total chemical sputtering yield exhibits a temperature maximum at about 650 K [161], which is substantially lower than the maximum of the methane production yield of 800 K (Fig. 18b) [161,215,216]. The product spectrum for chemical sputtering due to combined irradiation of graphite with H^0 and H^+ (Fig. 18b) also differs significantly from that of chemical erosion due to atomic hydrogen (Fig. 18a). For the latter, CH_4 is a minority species in the whole temperature range.

In contrast to *Haasz* and coworkers and *Vietzke* and coworkers, who measured hydrocarbon production yields by mass spectrometry [161,215,216] and molecular beam mass spectrometry [77,79,85], respectively (for description of the experimental setups see Sect. 4.2), *Hopf* and coworkers investigated the chemical sputtering of a-C:H films using in-situ real-time ellipsometry [141,142,217–219] (Sect. 4.3). This approach directly yields the total chemical sputtering yields but no information on the released species. In this view, it provides complementary information to the mass spectrometric investigations.

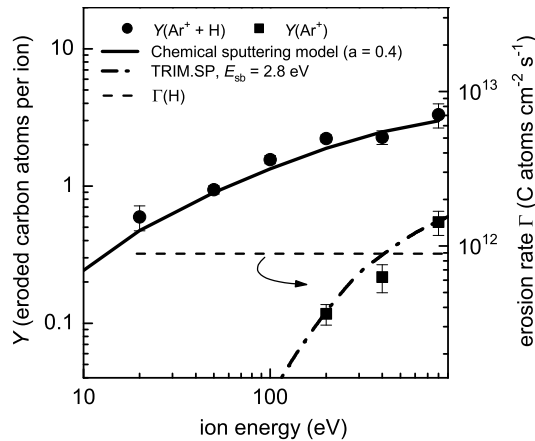


Fig. 19. Energy dependence of the erosion yield $Y(\text{Ar}^+)$ of physical sputtering of an a-C:H film by Ar^+ ions (*squares*) and the yield $Y(\text{Ar}^+ + \text{H})$ for chemical sputtering by a simultaneous flux of Ar^+ ions and hydrogen atoms (*circles*). The *dash-dotted line* shows the carbon physical sputtering yields as calculated by TRIM.SP [220] for sputtering by argon ions using a carbon surface-binding energy of $E_{\text{sb}} = 2.8$ eV. The *solid line* is the result of the chemical sputtering model by Hopf et al. [141]. The *dashed line* shows the absolute erosion rate (right-hand scale) by the applied flux of hydrogen atoms only. The surface temperature was about 340 K

Hopf et al. [141,142,217,218] investigated erosion of amorphous hydrogenated carbon (a-C:H) films due to combined Ar^+ ion and thermal atomic hydrogen atom impact in the low-temperature, low-energy regime. As discussed in Sect. 6.1.3, hard a-C:H films are a good model system for a graphite surface bombarded by hydrogen ions or a combination by arbitrary ions and atomic hydrogen. Hard a-C:H films were exposed to either one of the beams alone or to the combined Ar^+ ion and hydrogen atom beams. The experiments were performed at a surface temperature of about 340 K. The ion flux density was between 3 and $4 \times 10^{16} \text{ m}^{-2}\text{s}^{-1}$ and the hydrogen atom flux was $\sim 1.4 \times 10^{19} \text{ m}^{-2}\text{s}^{-1}$.

Figure 19 shows the erosion yield (per argon ion) as a function of ion energy. As all experiments involving ions were performed at approximately constant ion flux density, the yields on the left hand scale correspond roughly to the rates given on the right hand scale. The squares show the erosion by ions only. Physical sputtering is observed at energies of 200 eV and above. Below these energies the resulting rates are too low to be reliably detected in the experiment. For comparison, TRIM.SP [220] calculations were performed for a-C:H films with an H/(H+C) ratio of 0.3 using a surface binding energy of $E_{\text{sb}} = 2.8$ eV. This is shown as dash-dotted line. It is in good agreement with the experimental results.

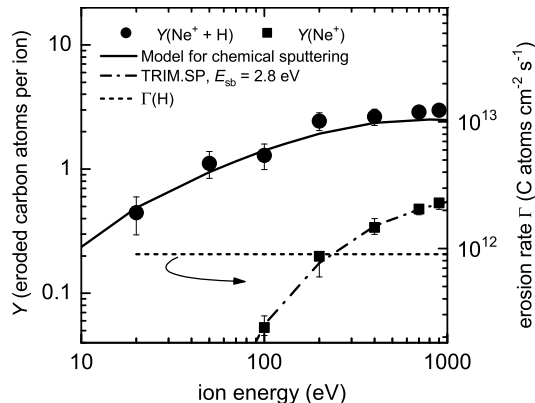


Fig. 20. Same as Fig. 19, but for neon ions

The erosion rate caused by the atomic hydrogen beam alone is shown as the dashed, horizontal line in Fig. 19. Since in the absence of ion bombardment it makes no sense to define an erosion yield (per ion) we can not compare the erosion yields, but we can compare the erosion rates (right-hand scale). For the used hydrogen atom flux the measured erosion rate of $\sim 5 \times 10^{15} \text{ m}^{-2} \text{ s}^{-1}$ results in an erosion yield per hydrogen atom (not per argon ion as the other yields in Fig. 19) of 6.4×10^{-4} .

If both beams interact simultaneously with the film the resulting erosion rate greatly exceeds the sum of physical sputtering and thermal chemical erosion; clearly a synergistic mechanism is active—*chemical sputtering*. The chemical sputtering yield decreases with decreasing energy. At the lowest energy being used, 20 eV, the measured rate is still a factor of 3 higher than the rate for pure chemical erosion by the hydrogen flux alone. For the case of simultaneous bombardment (hydrogen atoms and Ar^+ ions at 200 eV) the yield per hydrogen atom increases from 3.5×10^{-4} (no ions) to 3.5×10^{-3} . It can thus be concluded that the reactivity of the surfaces with atomic hydrogen is increased by a factor of 10, which is in good agreement with the findings of *Vietzke et al.* [77,85] and *Haasz et al.* [161,215,216]. This general result resembles that of erosion experiments applying energetic hydrogen isotopes [81], but, in contrast to these data, a clear decrease of the yield with decreasing ion energy is observed here. This is most probably due to the use of two separate beams and the fact that the atomic hydrogen flux is much higher than the ion flux. Based on these data, Hopf et al. suggested a microscopic model of chemical sputtering and devised a mathematical description of the energy dependence for this process. The model takes into account the damage produced by the impinging ions and the reaction of atomic hydrogen with this damage. The ion-induced damage is calculated with TRIM.SP.

The model is explained in detail in Sect. 7.2. The solid line in Fig. 19, which represents the result of this model, is in excellent agreement with the data.

The identical experiment was also performed for co-bombardment with neon ions and atomic hydrogen. The results are presented in Fig. 20 [219]. Remarkably, the model for chemical sputtering, which was developed for and fitted to the argon-hydrogen data, leads to a perfect description also of the neon-hydrogen data without any adjusted parameter.

6.3 Effect of Doping

The multi-step process of chemical erosion depends on a critical combination of hydrogen attachment and desorption and the thermal release of reaction products (Sect. 5.1). As the activation energies for the different processes are similar, small changes in the activation energies for hydrogen desorption and hydrocarbon radical release can strongly influence the resulting erosion yield.

It was observed already in the early years of research on chemical sputtering that additions of small quantities of impurity atoms to graphites can reduce the erosion yield. Dopants such as Fe, Ni, Ti, Mo, Si [221] and Ni [160] were shown to be effective, but most prominently boron additions almost completely suppressed chemical sputtering [221–223]. Even small amounts of B, for example = 0.5 at%, lead to a decrease of the temperature of hydrogen desorption [224] and, consequently, to a drastic reduction of chemical sputtering at elevated temperatures. As the activation energy for hydrogen desorption decreases below the activation energy for hydrocarbon radical emission, the reaction chain leading to erosion is interrupted [80,225].

Once the thermal chemical erosion is suppressed, other emission processes, which do not require elevated temperatures, are more readily distinguished. Fig. 21 shows the chemical sputtering yield of a 15 at% boron-doped pyrolytic graphite, USB15, as a function of temperature for different ion energies in comparison with high purity pyrolytic graphite [226]. At 1 keV, the chemical sputtering yield with a maximum at 800 K is almost completely suppressed, while for decreasing energy a low temperature process emerges which is active up to the temperature for hydrogen desorption. The activation energy for hydrogen desorption from USB15 was determined to about 1.2 eV. In contrast, pure graphite has an activation energy of 1.8 eV [80]. Chemical sputtering is possible up to temperatures where thermal release of hydrogen molecules sets in. The total chemical sputtering yield due to this low temperature process for deuterium ions at room temperature and 30 eV is about 3 at%. It remains constant down to 150 K [18,19,182].

The decrease of the chemical sputtering yield with boron doping has led to attempts to produce new graphitic materials with low erosion yield. Dopants, such as Si, Ti, V, Zr and W were added as carbide grains to carbon powder in the production process of fine grain graphites [17,227] and the chemical sputtering yield was studied using deuterium ions for 30 eV and 1 keV as a

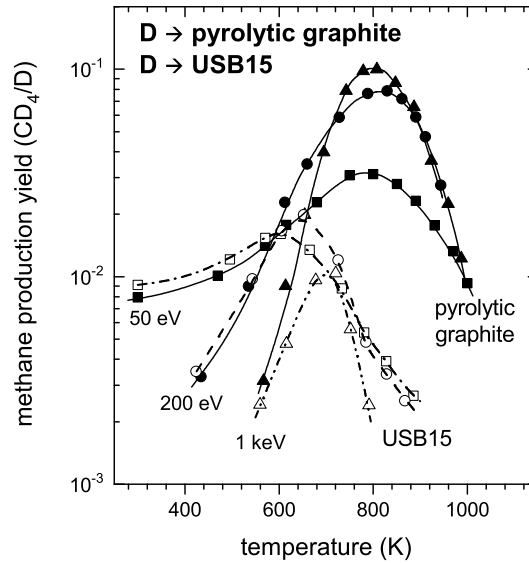


Fig. 21. Temperature dependence of the CD_4 production yield due to deuterium bombardment of pyrolytic graphite (solid symbols) and USB15 (open symbols) at different energies [226]

function of temperature, ion fluence, and grain size [228]. The effect of the dopants increased with decreasing carbide particle size. Finally, the addition of metallic dopants, such as titanium, vanadium, or tungsten, in atomic form by simultaneous sputter deposition of carbon and metal atoms, leads to doped carbon material with similar erosion behaviour as for boron doping [19,182]. For example, 3 at% W reduces the thermal erosion process as efficiently as 15 at% B [182]. For high ion fluences the preferential sputtering of carbon and the simultaneous enrichment of dopant particles leads to a development of a pronounced column-like surface structure and to an almost complete suppression of erosion below the threshold energy for sputtering of dopant atoms [228].

6.4 Chemical Sputtering with Molecular Ions at Low Energies

In recent years, much attention has been paid to determining chemical sputtering yields at room temperature and at very low energy. To achieve sufficiently high ion fluxes most researchers used molecular ion beams, i.e. H_2^+ and H_3^+ and the corresponding deuterated ions. The general assumption used in the evaluation of measured data is that a molecular ion is identical to the corresponding number of individual atoms impinging at the same velocity. This means that the energy is shared evenly between the constituents of the molecular ion, in other words, an H_2^+ ion is equivalent to two H^+ ions at

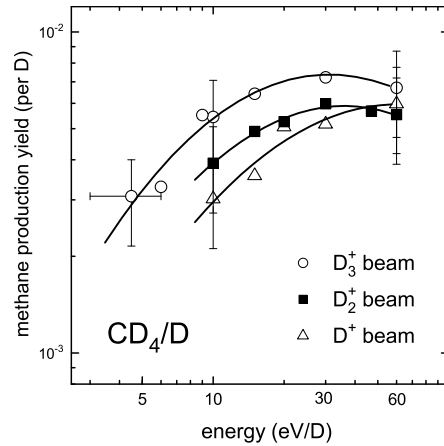


Fig. 22. Energy dependence of the methane production yield for sputtering of carbon with deuterium at room temperature [180]. Plotted is the yield per D atom for bombardment with D^+ , D_2^+ , and D_3^+ ions. For energies below 60 eV/D the measured yields start to deviate from each other. The lines are only a guide to the eye

half the energy and an H_3^+ ion equivalent to three H^+ ions at one third of the energy. This concept holds at high energies ($E >$ about 100 eV), but it breaks down at lower energies. This has been demonstrated by Yao et al. who investigated the physical sputtering of gold by N_2^+ and O_2^+ ions [229]. An enhancement of the measured sputtering yield per atom for N_2^+ compared to N^+ was observed for energies below 500 eV per projectile (i.e. 250 eV per atom). The difference increased with decreasing ion energy. At 50 eV per atom the N_2^+ yield is about a factor of 4 higher than the N^+ yield. For O_2^+ they found similar enhancements over O^+ for energies below 100 eV per atom.

For the chemical sputtering of carbon by D^+ , D_2^+ , and D_3^+ ions and energies below 60 eV per deuteron the methane production yields per deuteron for the three different ion species start to deviate (Fig. 22) [177–180]. The difference between these yields increases with decreasing energy per deuteron. The yield for D_2^+ is always higher than that for D^+ , and that for D_3^+ higher than that for D_2^+ . At the energy of 10 eV/D the D_3^+ yield is a factor of two higher than the D^+ yield. This effect has to be taken into account if experimental results at low ion energies are compared and different ion species have been used.

6.5 Summary of Experimental Results

Chemical sputtering depends on a variety of experimental parameters such as type of carbon material, sample temperature, ion energy, and ion flux.

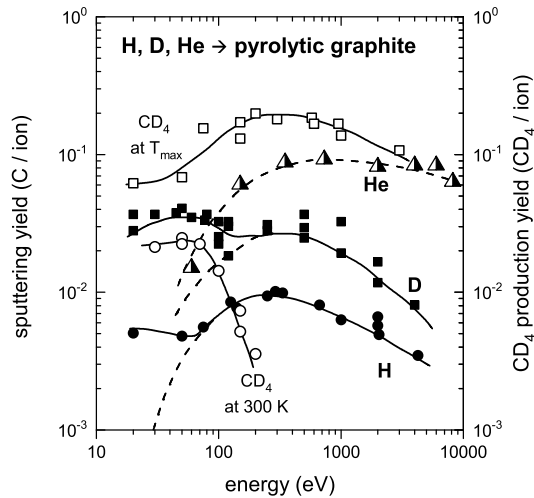


Fig. 23. Sputtering of carbon (pyrolytic graphite) with hydrogen, deuterium, and helium ions [173]. Comparison of weight loss data and CD_4 production. The dashed lines are predictions from an empirical formula for physical sputtering (see [173]). Solid lines are only a guide to the eye

These various parameters show strong, nonlinear interdependences so that a compact presentation of the physical and chemical dependences can be confusing at first glance. All relevant erosion processes (as defined in Sect. 3), i.e., physical sputtering, chemical erosion, and chemical sputtering can occur simultaneously. Which of them dominates the results depends on the experimental conditions. Strong interdependences exist between these processes. Furthermore, direct comparison of different experiments is difficult because in most cases more than one parameter is different. Nevertheless, the existing data base allows a rather advanced description of the physical and chemical processes and development of microscopic models for their interpretation. Before we start with a presentation of different models describing chemical sputtering, we want to make a critical assessment of the data, compare results from different methods, and summarize the most important points.

The energy dependence of sputtering of carbon materials with hydrogen ions differs from physical sputtering. The yield remains high at low energies, even below the threshold for physical sputtering (Figs. 12 and 23). The yield shows a strong isotope dependence (Figs. 12 and 23). At energies above about 100 eV yields for deuterium ions are a factor of 2-3 higher than those for hydrogen. The difference increases to about 5 to 7 for decreasing energies (below 100 eV). This is a proof that momentum transfer from the projectile ions to the target atoms, i.e., physical effects, plays an important role in this process. The difference between physical sputtering and chemical sputtering is nicely summarized in Fig. 23. Sputtering by helium ions leads to physical

sputtering. The measured weight loss data are in good agreement with an analytical prediction of physical sputtering shown by the line through the data points [173]. With decreasing energy the physical sputtering yield decreases strongly. For energies above about 100 eV the data for hydrogen and deuterium can also be well described by physical sputtering, but, in contrast to helium, their yields do not decrease with decreasing energy as anticipated for physical sputtering. They rather remain at relatively high values compared with physical sputtering. For the case of deuterium bombardment, the CD_4 production at 300 K, measured by a remote mass spectrometer, is also shown. Two points are remarkable: Firstly, at low energies, the yield is significantly lower than the weight loss data. This is due to the fact that CD_4 is not the only produced species. This point was discussed in Sect. 6.1.5. It underlines the fact that weight loss measurements provide the most reliable data for total sputtering yields. Secondly, at energies above about 80 eV the CH_4 production yield decreases strongly with increasing energy. This is in part due to the change of the product spectrum of released species which was also thoroughly discussed in Sect. 6.1.5. It is an indication that the dominant erosion processes below and above about 100 eV are different.

Fig. 23 also shows the enhanced CD_4 production yield at $T_{max} = 820$ K. At energies below about 100 eV the CD_4 production yield at 820 K is a factor of 3 higher than at 300 K and it is even higher than the weight loss measurements at 300 K. This higher chemical sputtering yield at T_{max} was also shown by weight loss data (see Fig. 12) and it is due to the temperature dependence of chemical sputtering (Sect. 6.1.1). The chemical sputtering yield increases with increasing temperature, shows a maximum around 800 K, and decreases for higher temperatures (Figs. 8 and 9). The exact position of the temperature maximum of the chemical sputtering yield depends on the ion flux (Sect. 6.1.4) and the ion energy (Sect. 6.1.2).

The chemical sputtering yield also shows a distinct flux dependence for ion fluxes higher than $10^{21} \text{ m}^{-2}\text{s}^{-1}$ (Sect. 6.1.4, Fig. 13). At these high fluxes, the maximum of chemical sputtering shifts to temperatures beyond 1000 K (see (6)). Since at such high temperatures the dominant process is hydrogen release the hydrocarbon yield is reduced.

Use of molecular ions at low energies leads to systematically different yields for different types of ions. The chemical sputtering yields per impinging D atom at the same energy per atom for bombardment with D^+ , D_2^+ , and D_3^+ start to depend on incident species below energies of about 60 eV per atom (Sect. 6.4, Fig. 22).

7 Mechanisms and Modelling for Chemical Sputtering

For the interaction of energetic hydrogen ions with carbon, it was found that the chemical reaction occurs after slowing down at the end of the range of the ions [85,125–127,195] impinging energetic hydrogen ions we can thus use

the following simple concept: As long as the projectiles are fast, chemical interactions with the target atoms are negligible and interaction with the target is dominated by kinetic processes, i.e., displacement of target atoms and physical sputtering. At the end of range, when the energetic particles are finally thermalised, they interact chemically with the target atoms. This chemical reaction at the end of the ion range can be described by the chemical erosion of carbon due to thermal hydrogen atoms. The first kinematic models of the reaction of atomic hydrogen with a carbon surface were proposed in the 1970s [10,230]. The most current and detailed one by *Küppers* et al. [157,155] was outlined in Sect. 5. The corresponding chemical erosion yield, Y_{therm} , is quantitatively described by (6). But, in addition to chemical erosion, effects due to the energetic ion impact have to be taken into account. These additional effects cause an enhancement of the yield due to

- radiation damage in the graphite lattice
- low temperature near-surface emission processes.

Further processes, which were shown to play a role in chemical sputtering by energetic ions are:

- diffusion of hydrocarbons from the end of range to the surface [124,125]
- the balance of formation and decomposition of hydrocarbons during irradiation [124,125] leading to transient effects at the start of the ion irradiation or after changing the temperature [44,124,125,231].

7.1 Empirical Analytic Description

Based on the just described simple concept of chemical sputtering, *Roth* and *García-Rosales* [159] suggested an empirical, analytical description which is capable of reproducing a variety of experimental observations. In particular, it describes the temperature, energy, flux, and isotope dependence of chemical sputtering.

7.1.1 Radiation Damage

Well-ordered graphitic structures provide only a very limited number of reaction sites for attack of atomic hydrogen. Although hydrogen atoms can form stable bonds with lattice atoms [232], chemical reactions occur only at edge atoms of graphitic planes [157]. Radiation damage (broken C–C bonds) provides additional reaction sites for hydrogen atoms, thus enhancing the chemical erosion yield. Radiation damage is created by kinetic-energy transfer from incident ions to lattice atoms (nuclear energy loss). It is responsible for the dependence of the chemical sputtering yield on ion energy and hydrogen isotope. To break a C–C bond a minimum energy has to be transferred to carbon lattice atoms. Therefore, this yield enhancement is characterized

by a threshold energy for damage production, E_{dam} . With increasing ion energy the total energy deposited in the target by nuclear collisions increases monotonically. However, the total energy deposited by nuclear collisions near the surface increases, reaches a maximum between 300 eV and 2 keV, and then decreases again. The chemical sputtering yield shows a similar energy dependence (see Figs. 10, 11, 14, and 15) as the energy deposited in the near-surface region. Thus it was concluded that the chemical sputtering yield is proportional to the energy deposited by nuclear collisions near the surface. The decrease of the chemical sputtering yield at higher energies indicates that energy deposition at large depths, typically beyond 200 nm, does not efficiently contribute to chemical sputtering. The effect of the damage production process is assumed to be similar to the physical sputtering process, but with a different threshold energy, E_{dam} . From a comparison of cross sections for damage production obtained by *Mech et al.* [233] with the analytic description of these processes analogous to physical sputtering (10), a value of 15 eV for E_{dam} , both for hydrogen and deuterium ions, was deduced.

Hence, this damage effect can be described by a multiplicative term to the basic chemical erosion yield, Y_{therm} (6), that includes a radiation damage yield, Y_{dam} ,

$$Y_{therm}^{damage} = Y_{therm} (1 + D \cdot Y_{dam}), \quad (8)$$

where D is a constant depending on the isotope mass of the bombarding particles. The numerical values for D are given in Tab. 2 (Sect. 7.1.3).

Below the threshold for damage production, the basic thermal reaction depends strongly on the crystalline perfection of the carbon material, with maximum yields between 10^{-4} for well annealed pyrolytic graphite and 10^{-1} for amorphous a-C:D layers [148]. At energies where radiation damage amorphises the graphite lattice, the dependence on the material structure disappears [78,148,162,166,168].

7.1.2 Low-temperature Near-surface Process, Y_{surf}

The mechanism for the low-temperature near-surface process, Y_{surf} , was deduced [159,176] by comparing the measured sputtering yields of carbon at room temperature due to H^+ and D^+ bombardment as a function of incident energy (see Fig. 12). The measured yields close to and below the threshold of physical sputtering (solid line in Fig. 12) are due to hydrocarbon formation. This formation cannot be explained by the reactions of the Küppers model, where a thermal activation at temperatures higher than 600 K is necessary for chemical erosion. Moreover, whereas the elementary reactions of the Küppers model do not show any isotope effect, a remarkable isotope effect (see Sect. 7.4) can be observed in the data plotted in Fig. 12. Based on this observation it was suggested that physical sputtering of weakly bound sp^3 CH_n groups from the surface is an explanation for Y_{surf} . The concentration

of these groups at the surface is high at room temperature under hydrogen bombardment, as demonstrated by *Küppers* and co-workers [157,158].

7.1.3 Empirical Roth-García-Rosales Formula

The total sputtering yield, Y_{tot} , for bombardment of a graphite surface with hydrogenic ions is given by the sum of physical sputtering, Y_{phys} , the chemical erosion enhanced by damage production, Y_{therm}^{damage} (8), and the near-surface process, Y_{surf} .

$$Y_{tot} = Y_{phys} + Y_{therm}(1 + DY_{dam}) + Y_{surf}, \quad (9)$$

where D is a parameter depending on the hydrogen isotope. For the physical sputtering yield for ions with energy E_0 the description by *Bohdansky* [234] is used

$$Y_{phys}(E_0) = QS_n(E_0) \left[1 - \left(\frac{E_{th}}{E_0} \right)^{2/3} \right] \left(1 - \frac{E_{th}}{E_0} \right)^2, \quad (10)$$

with

$$S_n(E_0) = \frac{0.5 \ln [1 + 1.2288 (E_0/E_{TF})]}{E_0/E_{TF} + 0.1728 \sqrt{E_0/E_{TF}} + 0.008 (E_0/E_{TF})^{0.1504}}. \quad (11)$$

Improvements included in the more recent description of physical sputtering by Eckstein and Preuss (see Chapter by Eckstein) are not significant in the context of chemical sputtering.

The thermal erosion yield at an ion flux, Φ , is obtained from

$$Y_{therm} = c^{sp^3} \frac{0.033 \cdot \exp(-E_{therm}/kT)}{2 \cdot 10^{-32} \Phi + \exp(-E_{therm}/kT)}, \quad (12)$$

with

$$c^{sp^3} = \frac{C \cdot (2 \cdot 10^{-32} \Phi + \exp(-E_{therm}/kT))}{2 \cdot 10^{-32} \Phi + [1 + \frac{2 \cdot 10^{29}}{\Phi} \exp(-E_{rel}/kT)] \exp(-E_{therm}/kT)}. \quad (13)$$

The factor C ,

$$C = \frac{1}{1 + (\Phi/[6 \times 10^{21}])^{0.54}}, \quad (14)$$

includes the dependence on ion flux, reducing the yield at fluxes above $6 \times 10^{21} \text{ m}^{-2}\text{s}^{-1}$. The chemical erosion at elevated temperature is enhanced by damage production given by

$$Y_{dam}(E_0) = QS_n(E_0) \left[1 - \left(\frac{E_{dam}}{E_0} \right)^{2/3} \right] \left(1 - \frac{E_{dam}}{E_0} \right)^2. \quad (15)$$

with $S_n(E_0)$ given by (11).

The surface erosion process is given by

$$Y_{surf}(E_0, T) = c^{sp^3} \frac{Y_{des}(E_0)}{\left(1 + e^{\frac{E_0 - 65 \text{ eV}}{40 \text{ eV}}}\right)} \quad (16)$$

with

$$Y_{des}(E_0) = QS_n(E_0) \left[1 - \left(\frac{E_{des}}{E_0}\right)^{2/3}\right] \left(1 - \frac{E_{des}}{E_0}\right)^2. \quad (17)$$

Although the detailed mechanism of the near-surface process is still under discussion, it is here assumed to scale as a physical sputtering term, but with reduced threshold energy, E_{des} . The denominator in (16) restricts the process to low energies, i.e., processes near the surface.

The parameters Q , E_{therm} , E_{th} , E_{dam} , E_{des} , E_{rel} , E_{TF} and D are given in Table 2 for the different hydrogen isotopes. Changes in the numerical values in (14) and (16) compared to [80,159] are introduced to smoothen the transition between different processes.

7.1.4 Comparison with Erosion Data

Fig. 24 shows the combined energy dependence of physical sputtering, chemical erosion, and chemical sputtering together with the analytic description developed on the basis of the results by *Küppers* et al. [155,157] for thermal hydrogen atoms and the inclusion of damage production and chemical

Table 2. Parameters for the empirical Roth–García-Rosales formula for the description of chemical sputtering by different hydrogen isotopes

Parameter	Hydrogen	Deuterium	Tritium
E_{TF}	415 eV	447 eV	479 eV
Q	0.035	0.1	0.12
E_{th}	31 eV	27 eV	29 eV
E_{dam}	15 eV	15 eV	15 eV
E_{des}	2 eV	2 eV	2 eV
D	250	125	83
E_{rel}	1.8 eV for pure carbon, 1.5 eV for Si, Ti, W doped carbon, 1.2 eV for B doped carbon		
E_{therm}	Gauss distribution of activation energies around 1.7 eV, $\sigma = 0.3$ eV		

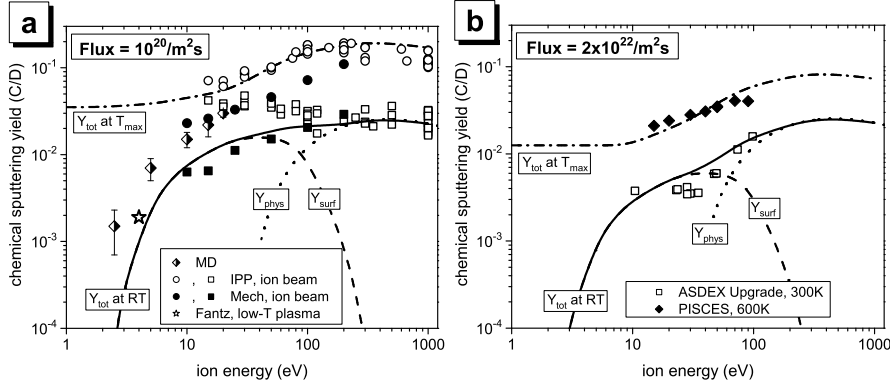


Fig. 24. Experimental data for the energy dependence of the erosion of graphite under D^+ bombardment as a function of energy compared to MD calculations and the analytical model [159,235]: a) for a flux of $10^{20} \text{ m}^{-2}\text{s}^{-1}$, b) for a flux of $2 \times 10^{22} \text{ m}^{-2}\text{s}^{-1}$. The data are from the following sources: MD [49], IPP [81], Mech [176], Fantz [106], ASDEX Upgrade [91], PISCES [104]. *Open symbols* are for weight loss and spectroscopic data, *solid symbols* for mass spectrometry.

sputtering by energetic ions [80,159]. The analytic description adequately describes the chemical erosion in its energy and temperature dependence.

As shown in Fig. 24a for deuterium, the formula leads to a good agreement with the available laboratory data (obtained for ion fluxes of the order of $10^{20} \text{ m}^{-2}\text{s}^{-1}$) for the energy dependence of the chemical sputtering yield at room temperature and close to T_{max} . The contributions of Y_{phys} and Y_{surf} are plotted separately. The experimental data shown are total sputtering yields obtained by weight loss measurements (open symbols) and mass spectrometry including higher hydrocarbons (solid symbols). Data at room temperatures and below 20 eV were obtained by MD simulations [49].

In Fig. 24b the analytical description is compared to the limited amount of data at an ion flux of about $10^{22} \text{ m}^{-2}\text{s}^{-1}$. The observed general decrease of the chemical sputtering yield is well reproduced by the flux dependence of the model.

7.1.5 Extrapolation to Thermal Energies

The experimental data for energetic ions extends only down to energies of 10 eV and has to be extrapolated to lower energies. At T_{max} the yield for chemical erosion due to exposure to thermal hydrogen depends strongly on the surface state of the material: for well annealed graphite surfaces exposed to H^0 , Y_{max} is of the order of 10^{-4} , while for the case of a-C:H layers or pre-irradiated graphite exposed to H^0 the erosion yields can reach 10^{-1} . For graphite irradiated simultaneously with H^0 and energetic ions (see Figs. 17

and 18) this yield is equivalent to the one for a-C:H layers [77–79,148,168] (see Sect. 6.1.3). For carbon surfaces in interaction with hydrogen plasmas, as e.g. in fusion applications, one has to assume that due to simultaneously incident energetic particles the plasma-facing surfaces are always amorphised and activated, such that the proposed equation predicts high, energy independent erosion yields Y_{therm} at T_{max} . In Fig. 24 it can be seen that using the analytical description for extrapolation of the chemical sputtering yield at T_{max} towards very low energies leads to values above 10^{-2} . For undamaged surfaces Y_{therm} may be an order of magnitude lower.

At room temperature measurements of chemical erosion due to exposure to thermal hydrogen show very low or no chemical erosion, depending on the actual structure of the carbon material. Therefore, the dominant erosion yield at low energies is Y_{surf} with a threshold energy around 2 eV and negligible yields at lower energies.

7.2 Chemical Sputtering Model by Hopf

Hopf et al. recently suggested a microscopic model for chemical sputtering of graphite with hydrogen ions at room temperature [141]. According to this concept, the key mechanisms are:

- Impinging ions break carbon-carbon bonds at the surface and within the ion penetration range.
- Locally available hydrogen reacts with these broken bonds forming C–H bonds.
- Consecutive C–C bond breaking and C–H bond formation processes lead to the production of stable, volatile hydrocarbon molecules at and below the surface (within the ion penetration range).
- Finally, the formed volatile hydrocarbon molecules diffuse to the surface and desorb. At room temperature, subsurface hydrocarbon species can desorb only from a limited near-surface layer.

Based on this microscopic concept, they devised a mathematical description of the energy dependence of chemical sputtering [236]. The impinging hydrogen ions provide both the damage (broken C–C bonds) and the chemically reactive species. The depth distributions of the broken C–C bonds, $y_{bb}^C(x, E)$, and the implanted species, $n(x, E)$, are calculated with TRIM.SP. The limitation of the out-diffusion of the molecules to a near-surface region is modelled by an exponentially decaying, depth-dependent probability for the out-diffusion, $\exp(-x/\lambda)$. The resulting contribution to the chemical sputtering yield due to formation of hydrocarbon species at room temperature, Y_{CH} , is given by the integral of the product of these three functions,

$$Y_{CH} = a \int y_{bb}^C(x, E) n(x, E) \exp(-x/\lambda) dx. \quad (18)$$

The parameter a is simply a scaling parameter. $y_{bb}^C(x, E)$ and $n(x, E)$ are both dependent on the ion energy and the mass of the impinging ions. The decay length of the out-diffusion probability is chosen as $\lambda = 0.4$ nm [236]. The energy required to break a C–C bond, E_{bb} , was chosen as 5 eV being a typical C–C bond energy. E_{bb} is an input parameter used for the TRIM.SP simulations. The surface binding energy of the hydrogen projectiles on graphite was approximated with the desorption energy of hydrogen from a fully hydrogen-covered graphite (0001) surface [237]. It becomes important at low energies because the projectile energy is increased by this amount when approaching the surface. The surface binding energy of carbon atoms was set to 7.4 eV [220]. Using these parameters, the chemical sputtering yield was calculated. The total sputtering yield, Y_{tot} , is given by the sum of the physical sputtering yield, Y_{phys} , and the contribution due to formation of hydrocarbons, Y_{CH} ,

$$Y_{tot} = Y_{phys} + Y_{CH}. \quad (19)$$

Y_{phys} is also calculated with TRIM.SP. Y_{tot} and the individual contributions of Y_{phys} and Y_{CH} (with $a = 1$) are shown in Fig. 25 together with experimental data from [81] for chemical sputtering at 300 K, which were already shown in Fig. 12. Considering the simplicity of the model, the agreement with the data is excellent. The model correctly describes the magnitude of the yield and the obvious isotope effect. It even reproduces details of the isotope effect (i.e., the ratio of the D^+ and H^+ yields). The hydrogen yield decreases slightly from 100 down to 15 eV while the deuterium yield actually increases in this range. This is reproduced by the model as well as the absolute difference between hydrogen and deuterium yields. The isotope effect and the fact that it is more pronounced at lower energies is discussed in Sect. 7.4.

This microscopic concept of the processes during chemical sputtering has some similarity to an earlier model where the chemical sputtering yield was scaled with the total nuclear energy deposition, i.e., the total energy transferred in projectile-target and target-target elastic collisions, in a near-surface layer [190]. But the observed large isotope effect at low energies requires that the term describing damage production must be associated with a process that has an threshold energy. If the total nuclear energy deposition instead of y_{bb}^C is used to describe the ion-induced damage in (18) a very different threshold behaviour occurs [236]. At energies above about 50 eV the choice of either total nuclear energy deposition or y_{bb}^C produces practically indistinguishable results, but below 50 eV y_{bb}^C leads to the decrease with decreasing energy as shown in Fig. 25, while the total nuclear energy deposition results in a monotonically increasing chemical sputtering yield with decreasing energy for both hydrogen isotopes [236].

The model by *Hopf* and coworkers [141] was originally developed for the combined irradiation of a-C:H films by energetic argon ions and thermal,

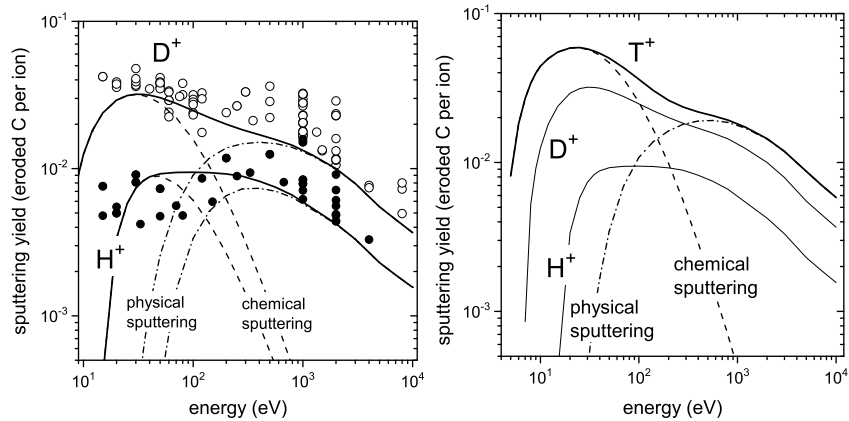


Fig. 25. *Left-hand side:* total sputtering yield of graphite bombarded with hydrogen or deuterium ions at room temperature as a function of ion energy. The *open* and *solid* symbols are measured yields taken from [81] for D^+ and H^+ bombardment, respectively. The *lines* show the physical sputtering yield calculated with TRIM.SP (*dash-dotted*), the chemical sputtering yield according to (18) (*dashed*), and the sum of chemical and physical sputtering (*solid*). *Right-hand side:* physical sputtering yield calculated with TRIM.SP (*dash-dotted*), chemical sputtering yield (18) (*dashed*), and total sputtering yield (19) (*solid*) for tritium. For comparison the total sputtering yields for hydrogen and deuterium from the *left side* are reproduced

atomic hydrogen (Sect. 6.2) [141,142,217–219] and had to be adapted to the case of bombardment of graphite with hydrogenic ions [236]. The main difference between the two cases is not the involved microscopic processes, but the source of the available hydrogen atoms. While for the hydrogen ion case, the projectile provides both damage and reactive species, for the co-bombardment case damage is produced by the argon ions and hydrogen is provided by the impinging atomic hydrogen flux. This leads to different depth distributions of the damage, $y_{bb}^C(x, E)$ and hydrogen densities.

For the hydrogen atom distribution in the target surface it was assumed that the density of hydrogen, and accordingly the probability that a reaction with a dangling bond occurs, decreases with increasing distance from the surface. This decay was described by an exponentially decaying function $\exp(-x/\lambda)$. The decay length was chosen to $\lambda = 0.4$ nm resulting in a maximum range of ~ 2 nm as found experimentally [89,238]. The chemical sputtering yield for the co-bombardment case is described by

$$Y_{CH} = a \int y_{bb}^C(x) \exp(-x/\lambda) dx, \quad (20)$$

where a is a scaling factor. The difference between (20) and (18) is that in (20) the term $n(x, E)$ is missing and the interpretation of $\exp(-x/\lambda)$ is different.

However, the interpretation of $\exp(-x/\lambda)$ as penetration for atomic hydrogen is, although intuitive, not unique. This was pointed out already in [141]. In light of the adaptation of this model to the hydrogen ion case it seems more appropriate to interpret $\exp(-x/\lambda)$ as the depth-dependent probability for out-diffusion of the formed volatile species. The model curves according to (20) are presented in Fig. 19 for $\text{Ar}^+ + \text{H}$ and in Fig. 20 for $\text{Ne}^+ + \text{H}$ as solid lines using $a = 0.4$ as scaling factor. Obviously the agreement with the data is very satisfying.

For the co-bombardment case, the chemical sputtering yield depends also on the incident atom-to-ion flux ratio. The flux dependence was investigated and discussed by *Hopf et al.* [141]. It was shown that a much higher atomic hydrogen flux compared with the ion flux is required to achieve maximal yields. In the $\text{Ar}^+ + \text{H}$ experiment the ratio of neutral hydrogen to argon ions was 400 [217,141] and even higher flux ratios are required for saturation of the process. A simple rate equation model to fit the experimentally observed flux dependence results in a saturation value for the chemical sputtering yield of about 3 (for Ar^+ ions at 200 eV) which is reached for flux ratios above 1000 [141]. This need for excess supply of atomic hydrogen can be understood taking into account that the dominant ion-induced process is displacement of bonded hydrogen [38]. This ion-induced depletion of hydrogen in the surface layer has to be balanced by the much higher influx of atomic hydrogen to keep the hydrogen concentration in the surface region high. *Hopf et al.* hypothesize that the flux ratio influences the fitting parameter a in (20), but this was not yet investigated in detail.

7.3 Molecular Dynamics Simulations

The chemical sputtering of carbon by hydrogen was also investigated in MD simulations in some detail by the Helsinki group [48–54,239–244]. *Salonen et al.* [239] studied the erosion of carbon by bombardment with hydrogen atoms at low energies (1 and 10 eV) but at high hydrogen fluxes. Atoms with 1 eV cause no carbon erosion, but at 10 eV some carbon erosion was observed. They also found that at very high fluxes carbon erosion is suppressed. They interpreted this effect as indicating that at high-flux hydrogen bombardment temporary supersaturation of hydrogen occurs at the surface. The high hydrogen content leads to the shielding of carbon atoms from new incoming hydrogen atoms, and thus a decrease of roughly one order of magnitude in the carbon erosion yield. They also found ejection of small hydrocarbon species (CH_y and C_2H_y). C_2H_y species contribute about 46% to the carbon removal rate.

In following investigations they identified a new sputtering mechanism which they named: ‘Swift Chemical Sputtering’ [48–53]. Swift chemical sputtering leads to the release of hydrocarbon radicals (including single C atoms) down to energies of 2 eV. Room temperature bombardment of an a-C:H

sample at 10 eV caused an erosion yield of 5×10^{-3} . With increasing temperature the yield increases, has a peak of about 0.02 at 900 K, and then decreases again [48]. This behaviour compares well with experimental results (see Sect. 6.1.1). The emitted species spectrum is dominated by CH_y and C_2H_y with a higher C_2H_y contribution at 900 K as compared to 300 K [49]. The energy dependence was studied in the interval from 1-35 eV [48,49]. The simulated yields for hydrogen, deuterium, and tritium are about a factor of 10 higher than the corresponding physical sputtering yields calculated by TRIM.SP. Furthermore, the simulations show a clear isotope effect increasing towards the threshold for chemical sputtering [49,51]. The yields for bombardment with tritium ions are consistently higher than those for deuterium, which in turn are higher than those for protium. These observations clearly support the picture that for chemical sputtering in this parameter range, i.e., 300 K and low energies (1-35 eV), chemical and physical interactions are of relevance.

The carbon erosion mechanism underlying the 'Swift Chemical Sputtering' process is the breaking of C-C bonds of surface hydrocarbon entities bonded to the network. These entities can be single carbon atoms or larger hydrocarbon groups. Since at these low energies the impinging atoms have not enough kinetic energy to physically sputter a carbon atom or a hydrocarbon group, the bond breaking takes place in a different manner. To break these bonds, ions penetrate the region directly between carbon atoms, i.e., they directly attack the covalent bond. The carbon atoms are then forced apart by the strong repulsive part of the potential energy function. This repulsion occurs very fast so that the surrounding carbon network does not have time to relax to a new equilibrium. The momentum transfer to the carbon atoms of the attacked covalent bond depends on the time the hydrogen atom spends between them. As a consequence, swift chemical sputtering can occur only in a certain incident energy range, so that it does not only have a low energy limit, but also a high energy limit. This is distinctly different than for the case of physical sputtering where only a low-energy limit (threshold energy) exists. This dependence on the interaction time offers also an explanation for the isotope dependence. As the velocity of different hydrogen isotopes changes according to the mass of the isotope, deuterium and tritium spend at the same incident energy more time between the carbon atoms than hydrogen. MD simulation have shown that the larger the mass of the hydrogen isotope, the larger the energy range where the bond breaking can occur is [52,53]. The 'Swift Chemical Sputtering' process, originally discovered for hydrogen bombardment of carbon, has recently been shown to occur also for bombardment with helium ions [54]. 'Swift Chemical Sputtering' is a new process which differs from usual physical sputtering and from chemical sputtering.

Recent simulations by *Krstić*, *Stuart* and *Reinhold* [245-248] have stressed the importance of preparing model surfaces by particle bombardment consistently with sputtering beam experiments. Self-consistent preparation of

carbon surfaces [245,248] by cumulative bombardment with the species (D, D₂, D₃), energy, and rovibrational-state-resolved projectiles led to improved agreement with measurements at 300 K [180] across the whole simulated energy range (7.5-30 eV/D), even at the level of partial hydrocarbon yields (methane, acetylene). Furthermore, it was shown [246] that chemical sputtering yields for molecular projectiles at impact energies below 15 eV/D exhibit a strong dependence on their initial, preimpact vibrational state. In fact, it was argued that resonant neutralization of the D₂⁺ ions used in experiments above the surface is expected to result in vibrationally excited D₂. Calculations using this assumption are found to be in better agreement with experiments for sputtering of methane [180] and acetylene [179] by D₂⁺ impact.

The atomistic nature of the MD modelling allows to identify the sputtered hydrocarbon species. The factor determining which type of hydrocarbon molecule is released is the depth of the broken C–C bond. The hydrocarbon chain above the broken bond leaves the surface. The predominantly eroded species are small hydrocarbons CH_y and C₂H_y, in agreement with experiments. Only a small fraction of heavier hydrocarbons are seen [49,241]. The composition of the released hydrocarbon flux changes with the structure of the a–C:H sample, with the incident energy, and with the type of hydrogen isotope. These changes are largest at very low energies (< 15 eV). Details can be found in [241]. Differences in the structure of the a–C:H sample can also lead to considerable differences in the total carbon erosion yield. The crucial factor is how many C–C bonds to the bulk and hydrocarbon groups an entity at the surface has. An entity with only one C–C bond to the surface erodes much easier than one with several bonds [48–50].

For low impact energies (<15 eV/D) CD_y and C₂D_y were found to be the dominant species [247]. The role of heavier hydrocarbons increases with energy, leading to substantial contributions of C₄D_y and C₅D_y at 30 eV/D impact energies. Energy spectra of the sputtered particles were found to be nearly independent of the mass of the sputtered particles or the impact energy: The average energy of the sputtered hydrocarbons is about 0.5 eV, indicating a kinetic desorption process [247].

To rule out a possible dependence of the MD results on the choice of the potential, MD simulations were conducted by the Helsinki group for three varieties of the empirical Brenner potential as well as in a tight-binding quantum-mechanical framework which is completely independent of the classical simulations [52,53]. It was shown that simulations with a quantum-mechanical treatment of the atomic system validate the bond breaking (and subsequently, erosion) mechanism, though the carbon sputtering yields given by the empirical and tight-binding models differ quantitatively.

MD at its present level is only capable of simulating a very short time after the impact, typical durations are of the order of a few picoseconds, but some simulations have been performed up to a few nanoseconds. This seems to be satisfactory at low impact energies (<30 eV/D), where the penetration depth

of the impact particle is small enough (< 1 nm) to allow sputtered particles to reach the surface through pores in the surface. For larger impact energies and accordingly deeper penetration of the projectiles, MD cannot describe any process that requires much longer time scales. Experiments by *Vietzke et al.* have, however, shown that a large fraction of the species is released with thermal energies and on a timescale of milliseconds [47]. In particular, MD can not describe the postulated processes of chemical sputtering as described in Sect. 7.2.

The characteristic time scale of the swift chemical sputtering process is of the order of 10 fs. The swift chemical sputtering process found in MD simulations and described above might be a good microscopic description of the surface process, Y_{surf} , postulated by *Roth et al.* [159] (see Sect. 7.1.2).

7.4 Isotope Effect

In the preceding discussion of mechanisms of chemical sputtering in many instances the isotope effect was mentioned. The importance of the isotope effect, i.e., the yield ratio Y_D/Y_H , for the understanding of the dominating mechanism is outlined in the following.

On the one hand, the chemical interaction of hydrogen isotopes with carbon is only weakly dependent on the isotope mass. Activation energies for hydrogen and deuterium desorption have been found to differ by less than 0.1 eV [155] and consequences for the thermally activated term of the chemical erosion yield, Y_{therm} , can, therefore, be neglected in (6). On the other hand, radiation damage and physical sputtering are certainly dependent on ion mass. The latter can be clearly seen in the experimental data on physical sputtering of carbon by H^+ and D^+ , where typically yields a factor of 2 higher are found for D^+ ions [81] (see solid lines in Fig. 12). Using TRIM.SP the physical sputtering yield has been calculated for T^+ . It turns out that the increase of physical sputtering from D^+ to T^+ is only small compared to the increase from H^+ to D^+ (Fig. 25b).

This leads to the expectation that also the chemical sputtering at elevated temperature and energies above 100 eV does not increase strongly from D^+ to T^+ . These expectations are corroborated by the first direct measurements of chemical sputtering with T^+ [249]. In fact, the chemical sputtering yield for tritium is the same as for deuterium within the uncertainties of the data.

The surface process Y_{surf} requires a bond-breaking process, both to form hydrocarbon reaction sites [141] and to release CH_n groups from the surface [49]. In this case, however, the damage production must occur within the first few monolayers of the solid and energies well below 100 eV play the dominant role. At energies close to the threshold for damage production, much stronger isotope effects must be expected. The simulation of the kinetic bond breaking process in MD calculations [49,245,247] indicates a threshold energy around 2 eV for D^+ . These predictions agree well with recent experimental data for CD_4 emission [177–180]. Also, *Salonen et al.* [49] found strong isotope

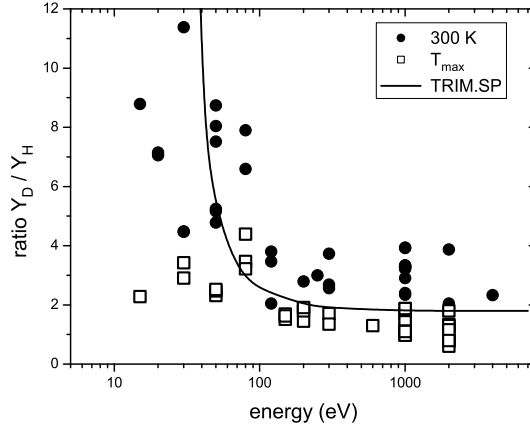


Fig. 26. Ratio of the chemical sputtering yield of graphite due to bombardment by D^+ and H^+ as a function of ion energy. Shown are the yields for bombardment at 300 K and at T_{max} (about 700 to 800 K) and results from TRIM.SP simulations of physical sputtering. The data are from [81]

effects in MD simulations in going from hydrogen to deuterium and tritium, increasing with decreasing energy.

The isotope effect and the fact that it is more pronounced at lower energies can, according to the Hopf model (Sect. 7.2), be explained by the following dependences:

(i) The collisional energy transfer is different for different projectile masses. The maximum transferrable energy in a head-on collision is given by the kinematic factor $\gamma(M_1, M_2) = 4M_1M_2/(M_1+M_2)^2$ where M_1 and M_2 are the projectile and target masses. For collisions with carbon the ratio of the kinematic factors for deuterium and protium projectiles is $\gamma(M_D, M_C)/\gamma(M_H, M_C) \approx 1.7$. Indeed, both in the experiment and in the TRIM.SP calculations a ratio $Y_{phys}(D)/Y_{phys}(H) \approx 2$ is found.

(ii) Due to the need to transfer a certain minimum amount of energy to a carbon atom to break a bond, $E_{bb} = 5$ eV in this case, there is an energy threshold $E_{th} = E_{bb}/\gamma(M_1, M_C)$ below which the chemical sputtering yield becomes zero. Small differences in the threshold energy between hydrogen, deuterium, and tritium will result in large isotope effects close to the threshold energy, as is observed for physical sputtering. This threshold is lower for D^+ than for H^+ . Consequently, the isotope effect increases when approaching the threshold from the high-energy side and becomes infinite below the threshold for protons.

Figure 26 shows a compilation of experimental data for the ratio of Y_{D^+}/Y_{H^+} for sputtering at room temperature and at T_{max} as a function of ion energy taking the total sputtering yield from weight loss data [81]. The thermal chemical erosion yield at T_{max} shows an isotope effect of the order

of a factor of 2, as predicted by the ratio of radiation damage production at high energies. In contrast, Y_{surf} measured at room temperature increases strongly towards low energies and a comparison with the isotope effect of physical sputtering, as obtained from TRIM.SP calculations, shows reasonable agreement. This comparison indicates that the threshold energies for hydrogen and deuterium, although being similar around 2 eV, differ clearly with slightly higher values for hydrogen. It can be expected that the threshold for tritium is even lower (see Fig. 25b) resulting in even higher isotope ratios Y_{T^+}/Y_{H^+} .

It is interesting to note that such high isotope ratios are not observed by residual gas analysis of the emitted stable hydrocarbons [250]. For stable hydrocarbons, which amount only to part of the total yield [81,245,247] ratios of the order of 2 were reported, similar to thermal hydrogen erosion. It may be speculated that stable hydrocarbons result from thermal emission, while the kinetic bond breaking processes result predominantly in the emission of radicals [49]. More investigations on the isotope effect, both experimentally and in MD simulations, will give valuable information of the underlying physical and chemical emission processes.

7.5 Effects due to Out-diffusion of Hydrocarbons

The fact that chemical erosion at elevated temperatures occurs at the end of the ion range requires that volatile reaction products diffuse to the surface, either through the crystalline lattice or along grain boundaries. The diffusion of reaction products has been inferred from transient effects after rapidly switching on or off the ion beam at constant surface temperature [124,125,251].

Figure 27 shows the CD_4 signal of a remote mass spectrometer during chemical sputtering of graphite at T_{max} using 8 keV D^+ as a function of time. When the beam is switched off, a sudden increase of the emission of hydrocarbons occurs before the mass spectroscopic signal decreases. In contrast, when the beam is switched back on during the decrease of the signal a transient drop of the signal is observed before the steady state emission is re-established [124]. The transients are more pronounced the higher the ion energy is between 8 keV D^+ and 100 keV D^+ [251]. These effects have been interpreted as the decomposition of reaction products by the incident ions during their diffusion to the surface, which reduces the hydrocarbon emission in steady state, but ends when the beam is turned off. Immediately after turning off the beam, a higher hydrocarbon emission results. From more detailed studies [124,125] a multi-region model for intra-granular diffusion and diffusion along grain boundaries was developed. Similar transients occur upon rapid changes in temperature and ion flux [44,231]. The study and interpretation of these transients can give more detailed insight into the chemical erosion process.

7.6 Summary

The different modelling approaches presented in this chapter serve different purposes. The empirical description (Roth–García-Rosales formula) was developed to provide an easy tool for predicting erosion rates in fusion devices. It allows to estimate erosion for a variety of parameters, such as temperature, energy of the impinging ions, ion flux, and isotope mass without detailed understanding of processes such as the flux dependence and near-surface emission.

The model by Hopf et al. (7.2, [141]) specialises on chemical sputtering at room temperature. It provides a microscopic explanation of the near-surface process Y_{surf} and, based on this, a mathematical model describing the energy dependence at room temperature. The Hopf model takes into account the depth distributions of the implanted hydrogen atoms and the radiation damage and the depth-dependent out-diffusion of the produced stable hydrocarbon species. It provides a deeper insight into the processes subsumed under the near-surface process, Y_{surf} , postulated in the empirical (Roth–García-Rosales formula). A key point of the Hopf model is that at room temperature out diffusion of produced hydrocarbon species is limited to a near-surface layer with a thickness of about 2 nm and it involves an energy threshold of about 5 eV given by the minimum energy required to break a carbon–carbon bond.

Even more basic physical understanding can be gained from MD simulations. Many elementary reaction and emission processes can be investigated

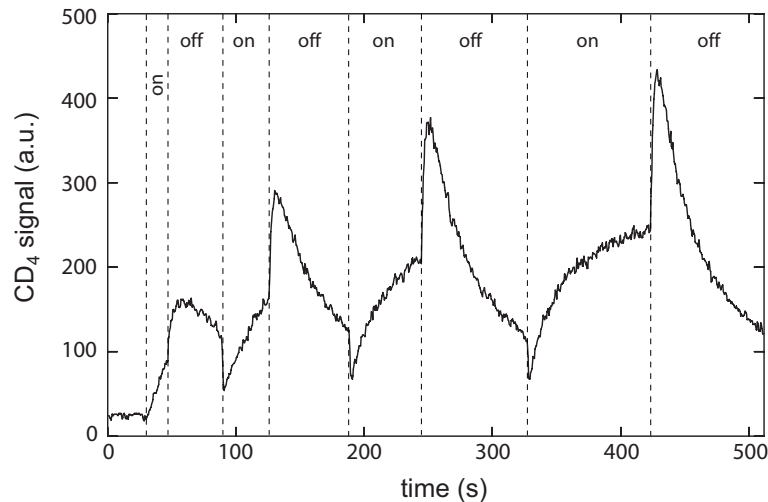


Fig. 27. Transient changes of the CD_4 signal of a remote mass spectrometer during chemical sputtering of graphite at T_{max} using 8 keV D^+ when switching on and off the incident ion beam [251]

in great detail. Due to technical restrictions in computing power, for the time being, only such processes which proceed on time scales below 1 ns can be evaluated. Thus MD simulations concentrate on kinetic emission processes, while thermal processes including particle diffusion cannot be accessed. The MD simulation suggest a threshold energy of about 2 eV for the near-surface process. Such a threshold is in accordance with recent experimental data for the energy dependence of the process down to 5 eV [177–180].

8 Chemical Sputtering with other Reactive Species

8.1 Oxygen

Oxygen as a highly reactive chemical species interacts strongly with carbon and carbonaceous materials. Molecular oxygen forms the gaseous products CO and CO₂ at elevated temperature, i.e., above ≈ 500 –800 K, depending on the specific carbon material [252–256]. The CO/CO₂ ratio increases substantially at higher temperatures and lower pressures [257]. More recently, *Stanmore* et al. [258] reviewed the gasification of carbon and the chemistry of combustion. They also report that the reaction rates are strongly influenced by the presence of impurities which, for example, may act as catalysts. Furthermore, the rates are influenced by the structure of the carbon material as was investigated in detail by *Müller* et al. [256] and *Balden* et al. [254]. For different graphites the yields typically range between 10^{-6} and 10^{-3} C/O₂ at 1000 K and at pressures between $\approx 10^{-5}$ mbar and atmospheric pressure [254,259]. At 2000 K yields of up to 10^{-2} have been measured [259]. In the case of thermal atomic oxygen the yields are substantially higher, as reported by *Rosner* and *Allendorf* [260]. The reaction yield increases with increasing temperature. It is about 0.08 at 700 K and reaches its maximum of about 0.6 around 1600 K.

If energetic oxygen ions impinge on carbon materials, the impinging oxygen is trapped or reemitted in the form of CO and CO₂ [261,262], while reemitted O and O₂ has not been found. At room temperature the saturation concentration of oxygen in graphite is 0.25 O/C [261,262]. It decreases with increasing temperature. For energies higher than 50 eV, the chemical sputtering yield at room temperature is around 0.7 removed C atoms per impinging O atom [261,263,262]. In the energy range from 50 eV to 10 keV, the energy dependence of the total carbon sputtering yield is rather weak [56,264,265,263]. The yield increases slightly with increasing energy. For energies higher than 500 eV, it is higher than 1 due to the increasing contribution of physical sputtering [56,261,263]. The maximum of the yield occurs at about 3 keV [56]. For energies lower than 50 eV, the yield decreases significantly.

Vietzke et al. [261] have also shown that the reactivity of thermal O₂ on graphite is enhanced by simultaneous argon ion bombardment at 5 keV. Furthermore, the ion bombardment makes the graphite surface reactive to O₂ even at room temperature. This interaction was recently also studied for

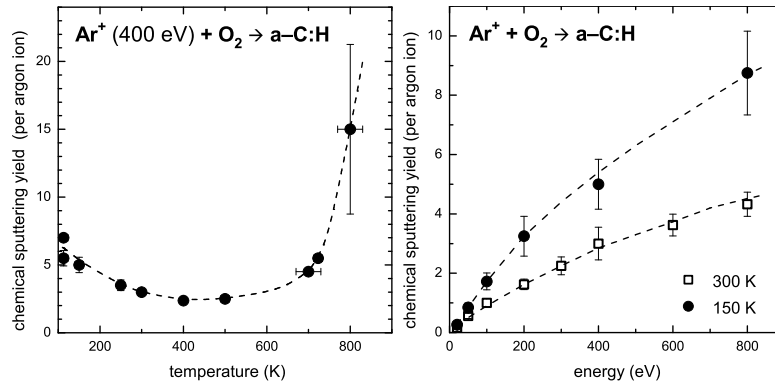


Fig. 28. Chemical sputtering of a-C:H films due to combined irradiation with Ar⁺ ions and molecular oxygen as a function of temperature (at a fixed ion energy of 400 eV) and ion energy (at 150 and 300 K) [266,267]. The *lines* are only a guide to the eye

a-C:H films in the low energy regime (20–800 eV) [266] using the MAJESTIX setup (see Sect. 4). While the physical sputtering yield for argon ions at 400 eV is about 0.3 (see Fig. 19), the chemical sputtering yield in the presence of molecular oxygen is about 3 removed carbon atoms per argon ion at room temperature (Fig. 28). The flux densities toward the sample surface in the experiment were approximately 4×10^{12} Ar⁺ cm⁻² s⁻¹ and 1×10^{16} O₂ cm⁻² s⁻¹. Obviously, the energy deposited by the incident ions causes reactions between oxygen and carbon. With increasing target temperature the yield increases to about 15 at 800 K due to an increasing contribution of thermally activated oxidation. Surprisingly, it also increases if the target temperature is decreased from room temperature to 110 K [267,266]. The latter observation can tentatively be explained as follows: Oxygen adsorbs at the surface into a weakly bound state. Incident ions cause chemical reactions of the adsorbed oxygen due to local heating and damage production, which lead to the formation of carbon oxides. With increasing temperature the desorption rate of the adsorbed oxygen increases, whereby the steady-state oxygen coverage decreases and, hence, the average number of oxides formed per incident ion decreases. The right-hand side of Fig. 28 shows the energy dependence. The chemical sputtering yield increases with increasing ion energy. This can be explained by increased energy deposition and damage production at the surface with increasing ion energy.

Besides these experiments with ion beams, a number of groups investigated the erosion of carbon and carbon films using oxygen-containing low-temperature plasmas [268–271]. In addition, several studies of plasma erosion of carbon films in fusion devices were conducted [272–277]. The interpretation of such experiments is complicated by the fact that many different species—

O^+ , O_2^+ , O_3^+ ions, O atoms, O_2 , and O_3 molecules and possibly other plasma ingredients—interact simultaneously with the surface. So far, not much is known about possible synergistic interactions, but the discussed particle-beam experiments for the co-bombardment with argon ions and molecular oxygen indicate that the ion- O_2 synergism may play a significant role in these plasma-erosion experiments. All of these experiments show consistently that very high erosion yields can be achieved with oxygen-containing plasmas. In fact, for the time being this is the most effective method for removing carbon and hydrocarbon layers. Furthermore, oxygen plasmas are used in the microelectronics industry for the ashing of photoresist [278] and the patterning of polymers [279].

8.2 Nitrogen

The erosion of carbon layers due to bombardment with nitrogen ions was investigated in a few ion beam experiments [280–283]. Sputtering of plasma-deposited, tetrahedrally coordinated amorphous carbon films (ta-C, a very dense and hard form of amorphous carbon) with N_2^+ ions at an energy of 1.5 keV gave yields between 0.54 (at 450 K) and 0.75 (at 1070 K) carbon atoms per nitrogen atom [281,282]. Furthermore, production of C_2N_2 was confirmed using a remote mass spectrometer [281,282]. Chemical sputtering of sputter-deposited amorphous carbon layers using 150 eV N_2^+ ions [283] resulted in a sputtering yield of ~ 0.5 per N_2^+ and the formation of C_2N_2 species by mass spectrometry was also observed. At this low energy, the physical sputtering calculated by TRIM.SP is well below 10^{-2} (see [280] and Fig. 3.9 in Chapter by Eckstein), so that chemical sputtering is the dominant

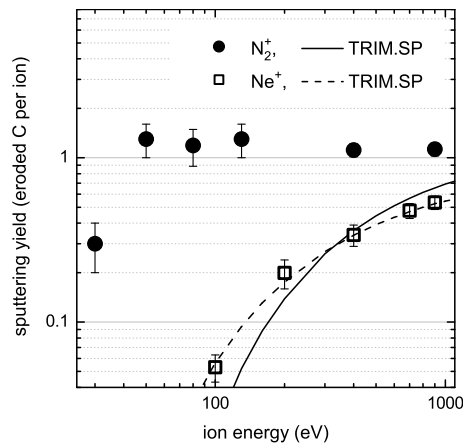


Fig. 29. Chemical sputtering of a-C:H films due to bombardment with N_2^+ compared with physical sputtering by Ne^+ ions [280] ($T = 340$ K)

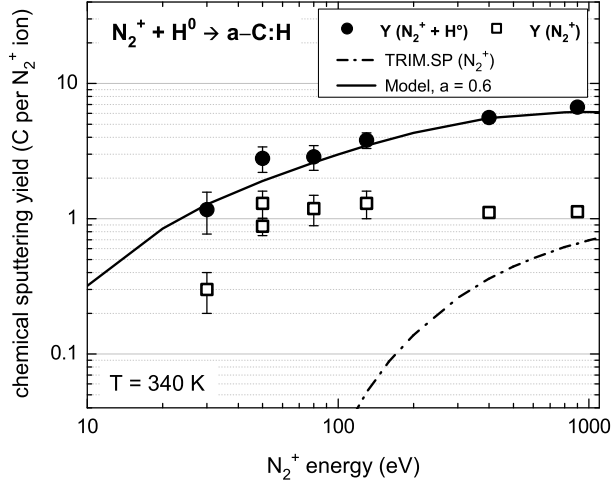


Fig. 30. Chemical sputtering of a-C:H films due to combined irradiation with hydrogen atoms and N_2^+ ions as a function of ion energy [284]. For comparison, the data for bombardment by N_2^+ ions alone are also shown. The *dash-dotted line* shows the prediction for physical sputtering due to N_2^+ ions alone, the *solid line* is the result of the chemical sputtering model with $a = 0.6$ (see (20) in Sect. 7.2)

erosion mechanism. The chemical sputtering yield of a-C:H layers by N_2^+ ion bombardment in the energy range between 50 and 900 eV is nearly constant at about 1 carbon per N_2^+ ion (Fig. 29) [280]. This value agrees well with the result of Grigull et al. [282], who found 0.5 C per N atom (which is equivalent to 1 per N_2^+ ion) for sputtering of ta-C films.

Chemical sputtering yields of hydrocarbon films due to combined irradiation with hydrogen atoms and N_2^+ ions [284] are shown in Fig. 30 together with the data for N_2^+ ions alone. The additional flux of hydrogen atoms causes a strong increase of the chemical sputtering yield. This is the highest yield per ion observed so far for such experiments. This can be attributed to three causes: i) two nitrogen atoms at half the ion energy arrive at the surface per N_2^+ ion, ii) due to the similar mass of nitrogen and carbon the energy transfer from nitrogen to carbon is very efficient. Both causes lead to a high density of broken bonds at or very close to the surface. iii) nitrogen alone shows already chemical sputtering (Fig. 29). This enhances the erosion additionally as compared with noble gas ions. The yield remains relatively constant if the sample is cooled from 340 K down to 120 K. [284]. This shows that at these temperatures thermal activation does not play a big role.

Besides these ion-beam experiments a number of investigations were carried out using nitrogen-containing plasmas for deposition of a-C:N:H films [285–293]. Trying to understand measured growth rates all authors came to the conclusion that chemical sputtering during deposition is an important

effect. In optical emission spectroscopy and mass spectrometry investigations of the gas phase in such plasmas, C–N species, predominantly C_2N_2 , were found [288–290,292].

Deposition of thin carbon nitride films was investigated by cathodic arc evaporation of a graphite cathode under simultaneous bombardment of the growing film by a nitrogen ion beam produced with a Kaufman-type ion source [286]. A reduction of the net carbon-deposition rate as a function of the energy of the additional nitrogen ion beam and as a function of increasing substrate temperature was found. This was interpreted as an additional chemical erosion mechanism and is obviously due to chemical sputtering by nitrogen ions [280]. Hong and Turban investigated the erosion of a–C:H films in nitrogen plasmas [288]. The erosion rate increases with increasing ion energy which is in reasonable agreement with the dual beam experiments [280,284]. They detected HCN and C_2N_2 by OES and mass spectrometry. With X-ray photoelectron spectroscopy they found the presence of 15–17% N in the near surface region after nitrogen plasma exposure.

The deposition and erosion of a–C:H layers was investigated in low-temperature plasmas using methane and hydrogen, respectively, with varying nitrogen addition [293]. The results are shown in Fig. 31. Already small additions of nitrogen to hydrogen cause a dramatic increase of the erosion rate if the ion energy, which is in this experiment defined by the substrate bias voltage, is higher than 30 eV. The erosion rate has a distinct maximum for a nitrogen addition of about 25% and decreases again for higher nitrogen fractions. In the whole mixture range the erosion rate is higher than in pure hydrogen or pure nitrogen plasmas. Because this effect strongly depends on the ion energy it has to be due to surface processes and cannot be explained by gas-phase reactions in the plasma. This enhancement of the erosion rate for hydrogen/nitrogen mixtures is due to the strong enhancement of the chemical sputtering yield for the combined interaction of atomic hydrogen and nitrogen ions that was observed in dual beam experiments (Fig. 30).

The right-hand side of Fig. 31 shows deposition and erosion rates of a–C:H layers in plasmas using different gas mixtures as a function of the substrate bias voltage, which is almost equivalent to the ion energy in this case. Methane (CH_4) leads to a relatively constant deposition rate of about 0.1 nm/s and hydrogen to a nearly constant erosion rate of about 0.02 nm/s in the whole investigated bias voltage range. The curve for H_2/N_2 (30% N_2 addition) shows a monotonic increase of the erosion rate with increasing bias voltage. The CH_4/N_2 (30% N_2 addition) mixture leads at low bias voltage to deposition which decreases with increasing bias voltage and then turns into erosion. The slope is similar to that of the H_2/N_2 curve. This change over from deposition to erosion is caused by the increasing chemical sputtering yield with increasing bias voltage.

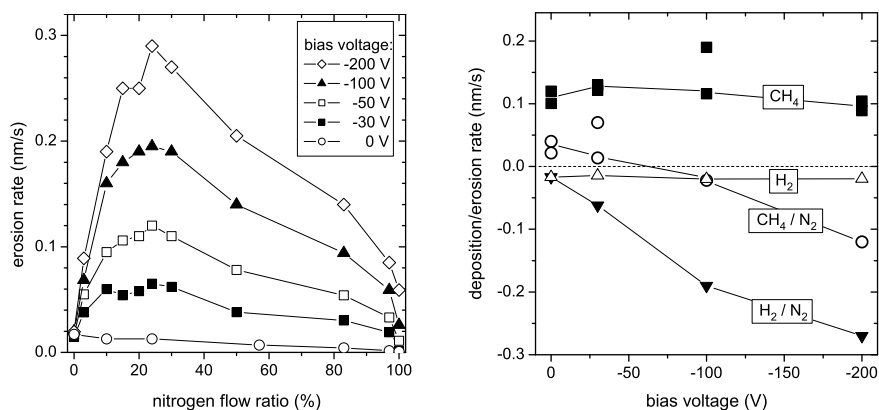


Fig. 31. Erosion and deposition of a-C:H layers in nitrogen containing plasmas. *Left-hand side:* Erosion rates of a-C:H layers in plasmas using H₂/N₂ gas mixtures as a function of the N₂ addition for different bias voltages (the bias voltage defines the ion energy). *Right-hand side:* Deposition and erosion rates of a-C:H layers in plasmas using different gas mixtures as a function of the substrate bias voltage [293]. The nitrogen admixture to H₂ and CH₄ was 30%. *Lines* are only a guide to the eye

8.3 Fluorine

Etching of carbon layers by fluorine atoms is an important process in microelectronics. The plasma chemistry in the etching of silicon and silicon oxide is controlled in such a way that polymeric fluoro-carbon layers are deposited on the side walls of the etched features. These deposits have to be removed in the following processing step. Therefore, the related plasma-surface-interaction processes have been studied in great detail [294–299]. On the other hand, if carbon or hydrocarbon films are etched in fluorine-containing plasmas, a CF surface layer is built up at the very surface, so that the aforementioned processes are also relevant for the etching (chemical sputtering) of carbon.

References

1. V. Kohlschütter: *Jahrb. Radioakt.* **9**, 355 (1912)
2. A. Güntherschulze: *Z. Phys.* **36**, 563 (1926)
3. W. Hauffe: In *Sputtering by Particle Bombardment III*, ed. by R. Behrisch, K. Wittmaack, *Top. Appl. Phys.* **64**, 305 (1991), Russ. translation: (MIR, Moscow 1998)
4. J.W. Coburn, H.F. Winters: *J. Vac. Sci. Technol.* **16**, 391 (1979)
5. H.F. Winters, J.W. Coburn: *Appl. Phys. Lett.* **34**, 70 (1979)
6. J. Winter: *J. Nucl. Mater.* **161**, 265 (1989)
7. J. Roth, J. Bohdansky, W. Poschenrieder, M.K. Sinha: *J. Nucl. Mater.* **63**, 222 (1976)
8. S.K. Erents, C.M. Braganza, G.M. McCracken: *J. Nucl. Mater.* **63**, 399 (1976)
9. N.P. Busharov, E.A. Gorbato, V.M. Gusev, M.I. Guseva, Y.V. Martynenko: *J. Nucl. Mater.* **63**, 230 (1976)
10. M. Balooch, D.R. Olander: *J. Chem. Phys.* **63**, 4772 (1975)
11. L. Zielinski, G.C. Schwartz: In *Electrochem. Soc. Abstracts* **75**, 117 (1975)
12. M. Armacost, P.D. Hoh, R. Wise, W. Yan, J.J. Brown, J.H. Keller, G.A. Kaplita, S.D. Halle, K.P. Muller, M.D. Naeem, S. Srinivasan, H.Y. Ng, M. Gutsche, A. Gutmann, B. Spuler: *IBM J. Res. Dev.* **43**, 39 (1999)
13. J.P. Chang, J.W. Coburn: *J. Vac. Sci. Technol.* **21**, 145 (2003)
14. T.A. Burtseva, O.K. Chugunov, E.F. Dovguchits, V.L. Komarov, I.V. Mazul, A.A. Mitrofansky, M.I. Persin, Y.G. Prokofiev, V.A. Sokolov, E.I. Trofimchuk, L.P. Zav'jalsky: *J. Nucl. Mater.* **191–194**, 309 (1992)
15. C. García-Rosales, W. Eckstein, J. Roth: *J. Nucl. Mater.* **218**, 8 (1994)
16. E. Vietzke, A.A. Haasz: In *Physical Processes of the Interaction of Fusion Plasmas with Solids*, ed. by W.O. Hofer, J. Roth (Academic, New York 1996), pp. 135
17. C. García-Rosales, M. Balden: *J. Nucl. Mater.* **290–291**, 173 (2001)
18. E. de Juan Pardo, M. Balden, B. Ciecwiwa, C. García-Rosales, J. Roth: *Phys. Scripta* **T111**, 62 (2005)
19. M. Balden, C. Adelhelm, E. de Juan Pardo, J. Roth: *J. Nucl. Mater.* **363–365**, 1173 (2007)
20. P. Sigmund, A. Gras-Marti: *Nucl. Instrum. Meth.* **168**, 389 (1980)
21. A. Gras-Marti, P. Sigmund: In *Proc. Symp. on Sputtering (SOS)*, ed. by P. Varga, G. Betz, E.P. Viehböck (Techn. Univ. Wien, Vienna 1980), pp. 512
22. U. Littmark, W.O. Hofer: *Nucl. Instrum. Meth.* **168**, 329 (1980)
23. K. Schmid, J. Roth, W. Eckstein: *J. Nucl. Mater.* **290–293**, 148 (2001)
24. K. Schmid, J. Roth: *J. Nucl. Mater.* **302**, 96 (2002)
25. O. Almén, G. Bruce: *Nucl. Instrum. Meth.* **11**, 279 (1961)
26. R.A. Zuhr, J. Roth, W. Eckstein, U. von Toussaint, J. Luthin: *J. Nucl. Mater.* **290–293**, 162 (2001)
27. K. Schmid, J. Roth: *Surf. Coat. Technol.* **158**, 81 (2002)
28. K. Schmid, J. Roth: *J. Nucl. Mater.* **313–316**, 302 (2003)
29. C. Linsmeier, J. Roth, K. Schmid: *Atomic and Plasma-Material Interaction Data for Fusion* **12**, 79 (2003)
30. K. Schmid, M. Baldwin, R. Doerner: *J. Nucl. Mater.* **337–339**, 862 (2005)
31. M.J. Baldwin, R.P. Doerner, D. Nishijima, K. Schmid, D.G. Whyte, J.G. Kulpin, G. Wright: *J. Nucl. Mater.* **358**, 96 (2006)

32. W.D. Sproul, D.J. Christie, D.C. Carter: *Thin Solid Films* **491**, 1 (2005)
33. D.M. Manos, D.L. Flamm (Eds.): *Plasma Etching: An Introduction* (Academic, San Diego 1989)
34. O. Auciello, D.E. Ibbotson, D.L. Flamm: *Nucl. Instrum. Meth. B* **23**, 419 (1987)
35. H.F. Winters, J.W. Coburn: *Surf. Sci. Rep.* **14**, 161 (1992)
36. J. Roth: In *Sputtering by Particle Bombardment II*, ed. by R. Behrisch, *Top. Appl. Phys.* **52**, 91 (1983), Russ. translation: (MIR, Moscow 1986)
37. J.W. Davis, A.A. Haasz: *Appl. Phys. Lett.* **57**, 1976 (1990)
38. W. Jacob: *Thin Solid Films* **326**, 1 (1998)
39. J.W. Coburn, H.F. Winters: *J. Appl. Phys.* **50**, 3189 (1979)
40. E.P. Vaulin, N.E. Georgieva, T.P. Martynenko, L.V. Feoktistov: *Sov. J. Plasma Phys.* **7**, 23 (1981)
41. R.P. Doerner, S.I. Krasheninnikov, K. Schmid: *J. Appl. Phys.* **95**, 4471 (2004)
42. K. Schmid, M. Baldwin, R. Doerner: *J. Nucl. Mater.* **348**, 294 (2006)
43. J. Roth: *J. Nucl. Mater.* **103**, 291 (1982)
44. J. Roth, J. Bohdanský, K.L. Wilson: *J. Nucl. Mater.* **111–112**, 775 (1982)
45. V. Philipps, K. Flaskamp, E. Vietzke: *J. Nucl. Mater.* **111–112**, 781 (1982)
46. J. Roth, W. Möller: *Nucl. Instrum. Meth. B* **7–8**, 788 (1985)
47. E. Vietzke: *J. Nucl. Mater.* **290–293**, 158 (2001)
48. E. Salonen, K. Nordlund, J. Keinonen, C. Wu: *Europhys. Lett.* **52**, 504 (2000)
49. E. Salonen, K. Nordlund, J. Keinonen, C. Wu: *Phys. Rev. B* **63**, 195415 (2001)
50. E. Salonen, K. Nordlund, J. Keinonen, C. Wu: *J. Nucl. Mater.* **290–293**, 144 (2001)
51. K. Nordlund, E. Salonen, J. Keinonen, C. Wu: *Nucl. Instrum. Meth. B* **180**, 77 (2001)
52. A. Krasheninnikov, E. Salonen, K. Nordlund, J. Keinonen, C. Wu: *Contrib. Plasma Phys.* **42**, 451 (2002)
53. A. Krasheninnikov, K. Nordlund, E. Salonen, J. Keinonen, C. Wu: *Computational Mater. Sci.* **25**, 427 (2002)
54. K. Nordlund: *Nucl. Instrum. Meth. B* **218**, 9 (2004)
55. J. Roth, J. Bohdanský, A.P. Martinelli: *Radiat. Eff. Def. Sol.* **48**, 213 (1980)
56. E. Hechtel, J. Bohdanský, J. Roth: *J. Nucl. Mater.* **103**, 333 (1981)
57. G. Sauerbrey: *Zeitschrift für Physik* **155**, 206 (1959)
58. M.C. Chuang, J.W. Coburn: *J. Vac. Sci. Technol. A* **8**, 1969 (1990)
59. G. Hayderer, M. Schmid, P. Varga, H. Winter, F. Aumayr: *Rev. Sci. Instrum.* **70**, 3696 (1999)
60. J. Bohdanský, J. Roth, M.K. Sinha, W. Ottenberger: *J. Nucl. Mater.* **63**, 115 (1976)
61. H.L. Bay, J. Roth, J. Bohdanský: *J. Appl. Phys.* **48**, 4722 (1977)
62. R. Behrisch, J. Roth, J. Bohdanský, A. Martinelli, B. Schweer, D. Rusbüldt, E. Hintz: *J. Nucl. Mater.* **93–94**, 645 (1980)
63. A.A. Haasz, P.C. Stangeby, O. Auciello: *J. Nucl. Mater.* **111–112**, 757 (1982)
64. O. Auciello, A.A. Haasz, P.C. Stangeby: *Phys. Rev. Lett.* **50**, 783 (1983)
65. P.C. Stangeby, O. Auciello, A.A. Haasz: *J. Vac. Sci. Technol. A* **1**, 1425 (1983)
66. J. Roth, C. Hopf: *J. Nucl. Mater.* **334**, 97 (2004)
67. A. Nerken, L.C. Beavis, K. Bhagwan Das, R. Grande, D.H. Holekeboer, J.E. McRea, D. Patterson, E. Stroebelt, P. Varadi: *J. Vac. Sci. Technol.* **9**, 1260 (1972)

68. J.A. Basford, M.D. Boeckmann, R.E. Ellefson: *J. Vac. Sci. Technol. A* **11**, 22 (1993)
69. D.J. Dagel, C.M. Mallouris, J.R. Doyle: *J. Appl. Phys.* **79**, 8735 (1996)
70. R. Dobrozemsky: *J. Vac. Sci. Technol.* **9**, 220 (1972)
71. T. Schwarz-Selinger, R. Preuss, V. Dose, W.v.d. Linden: *J. Mass Spectrom.* **36**, 866 (2001)
72. H.D. Kang, R. Preuss, T. Schwarz-Selinger, V. Dose: *J. Mass Spectrom.* **37**, 748 (2002)
73. U. von Toussaint, V. Dose, A. Golan: *J. Vac. Sci. Technol. A* **56**, 401 (2004)
74. T. Zecho, B.D. Brandner, J. Biener, J. Küppers: *J. Phys. Chem. B* **105**, 6194 (2001)
75. T. Zecho, B.D. Brandner, J. Biener, J. Küppers: *J. Phys. Chem. B* **106**, 610 (2002)
76. V. Philipps, E. Vietzke, M. Erdweg, A. Flaskamp: *J. Nucl. Mater.* **145-147**, 292 (1987)
77. E. Vietzke, K. Flaskamp, V. Philipps: *J. Nucl. Mater.* **111-112**, 763 (1982)
78. E. Vietzke, V. Philipps, K. Flaskamp, C. Wild: In *Amorphous hydrogenated carbon films*, ed. by P. Koidl, P. Oelhafen (Les Éditions de Physique, Les Ulis 1987), p. 351
79. E. Vietzke, V. Philipps, K. Flaskamp: *J. Nucl. Mater.* **162-164**, 898 (1989)
80. J. Roth: *J. Nucl. Mater.* **266-269**, 51 (1999)
81. M. Balden, J. Roth: *J. Nucl. Mater.* **280**, 39 (2000)
82. T. Schwarz-Selinger: to be submitted to *Plasma Sources Sci. Technol.* (2007)
83. W. Walcher: *Z. Physik* **122**, 62 (1944)
84. J. Benedikt, S. Agarwal, D.J. Eijkman, W. Vandamme, M. Creatore, M.C.M. van de Sanden: *J. Vac. Sci. Technol. A* **23**, 1400 (2005)
85. E. Vietzke, K. Flaskamp, V. Philipps: *J. Nucl. Mater.* **128-129**, 545 (1984)
86. R.M.A. Azzam, N.M. Bashara: *Ellipsometry and polarized light*, 1st edn. (Elsevier, Amsterdam 1977)
87. R.W. Collins: *Materials Science Forum* **52&53**, 341 (1989)
88. A. von Keudell, W. Jacob, W. Fukarek: *Appl. Phys. Lett.* **66**, 1322 (1995)
89. A. von Keudell, W. Jacob: *J. Appl. Phys.* **79**, 1092 (1996)
90. A. von Keudell, W. Jacob: *J. Appl. Phys.* **81**, 1531 (1997)
91. A. Kallenbach, A. Thoma, A. Bard, K.H. Behringer, K. Schmidtman, M. Weinlich, ASDEX Upgrade Team: *Nucl. Fusion* **38**, 1097 (1998)
92. A. Kallenbach, A. Bard, A. Carlson, R. Dux, the ASDEX Upgrade Team: *Phys. Scripta* **T81**, 43 (1999)
93. M.F. Stamp, S.K. Erents, W. Fundamenski, G.F. Matthews, R.D. Monk: *Phys. Scripta* **T91**, 13 (2001)
94. M.F. Stamp, S.K. Erents, W. Fundamenski, G.F. Matthews, R.D. Monk: *J. Nucl. Mater.* **290-293**, 321 (2001)
95. D.G. Whyte, W.P. West, C.P.C. Wong, R. Bastasz, J.N. Brooks, W.R. Wampler, N.H. Brooks, J.W. Davis, R.P. Doerner, A.A. Haasz, R.C. Isler, G.L. Jackson, R.G. Macaulay-Newcombe, M.R. Wade: *Nucl. Fusion* **41**, 1243 (2001)
96. S. Brezinsek, P.T. Greenland, P. Mertens, A. Pospieszczyk, D. Reiter, U. Samm, B. Schweer, G. Sergienko: *J. Nucl. Mater.* **313-316**, 967 (2003)
97. S. Brezinsek, P. Mertens, A. Pospieszczyk, G. Sergienko, U. Samm: *Phys. Scripta* **T103**, 51 (2003)

98. S. Brezinsek, A. Huber, S. Jachmich, A. Pospieszczyk, B. Schweer, G. Sergienko: *Fusion Sci. Technol.* **47**, 209 (2005)
99. S. Brezinsek, A. Pospieszczyk, M.F. Stamp, A. Meigs, A. Kirschner, A. Huber, P. Mertens: *J. Nucl. Mater.* **337–339**, 1058 (2005)
100. S. Brezinsek, G. Sergienko, A. Pospieszczyk, P. Mertens, U. Samm, P.T. Greenland: *Plas. Phys. Contr. Fusion* **47**, 615 (2005)
101. M.F. Stamp, P. Andrew, S. Brezinsek, A. Huber: *J. Nucl. Mater.* **337–339**, 1038 (2005)
102. R. Pugno, K. Krieger, A. Kirschner, A. Kallenbach, D. Coster, R. Dux, U. Fantz, J. Likonen, H.W. Müller, J. Neuhauser, V. Rohde, E. Vainonen-Ahlgren, ASDEX Upgrade Team: *J. Nucl. Mater.* **337–339**, 985 (2005)
103. U. Fantz, S. Meir, ASDEX Upgrade Team: *J. Nucl. Mater.* **337–339**, 1087 (2005)
104. D. Whyte, G. Tynan, R. Doerner, J. Brooks: *Nucl. Fusion* **41**, 47 (2001)
105. H. Grote, W. Bohmeyer, P. Kornejew, H.D. Reiner, G. Fussmann, R. Schlögl, G. Weinberg, C.H. Wu: *J. Nucl. Mater.* **266–269**, 1059 (1999)
106. U. Fantz, H. Paulin: *Phys. Scripta* **T91**, 25 (2001)
107. U. Fantz: *Contrib. Plasma Phys.* **44**, 508 (2004)
108. U. Fantz: *Nuclear Fusion Research – Understanding Plasma–Surface Interaction*, Springer Series in Chemical Physics (Springer, Berlin 2005) pp. 99
109. P. Starke, U. Fantz, M. Balden: *J. Nucl. Mater.* **337–339**, 1005 (2005)
110. K. Behringer, H.P. Summers, B. Denne, M. Forrest, M. Stamp: *Plas. Phys. Contr. Fusion* **31**, 2059 (1989)
111. A. Pospieszczyk, Y. Ra, Y. Hirooka, R.W. Conn, D.M. Goebel, B. LaBombard, R.E. Nygren, Spectroscopic Studies of Carbon Containing Molecules and their Break-up in Pisces-A (UCLA Report PPG-1251, 1989).
112. S. Brezinsek, A. Pospieszczyk, A. Kirschner, G. Sergienko, A. Huber, V. Philipps, P. Mertens, U. Samm, M.F. Stamp, A. Meigs, P.T. Greenland, JET-EFDA contributors: *Phys. Scripta* **T111**, 42 (2004)
113. V. Philipps, M. Stamp, A. Pospieszczyk, A. Huber, A. Kirschner, E. Vietzke: *J. Nucl. Mater.* **313–316**, 354 (2003)
114. J. Perrin, Y. Takeda, N. Hirano, Y. Takeuchi, A. Matsuda: *Surf. Sci.* **210**, 114 (1989)
115. A. Matsuda, K. Nomoto, Y. Takeuchi, A. Suzuki, Y. Yuuki, J. Perrin: *Surf. Sci.* **227**, 50 (1990)
116. D.A. Doughty, J.R. Doyle, G.H. Lin, A. Gallagher: *J. Appl. Phys.* **67**, 6220 (1990)
117. A. Nuruddin, J.R. Doyle, J.R. Abelson: *J. Appl. Phys.* **76**, 3123 (1994)
118. C. Hopf, K. Letourneur, W. Jacob, T. Schwarz-Selinger, A. von Keudell: *Appl. Phys. Lett.* **74**, 3800 (1999)
119. C. Hopf, T. Schwarz-Selinger, W. Jacob, A. von Keudell: *J. Appl. Phys.* **87**, 2719 (2000)
120. W. Jacob, C. Hopf, A. von Keudell, T. Schwarz-Selinger: In *Hydrogen Recycling at Plasma Facing Materials*, ed. by C.H. Wu, (Kluwer, Dordrecht 2000), pp. 331
121. E. Vietzke, K. Flaskamp, M. Hennes, V. Philipps: *Nucl. Instrum. Meth. B* **2**, 617 (1984)
122. A.A. Haasz, J.W. Davis: *Nucl. Instrum. Meth. B* **83**, 117 (1993)
123. J.W. Davis, A.A. Haasz, C.H. Wu: *J. Nucl. Mater.* **196–198**, 581 (1992)

124. S. Chiu, A.A. Haasz, P. Franzen: *J. Nucl. Mater.* **218**, 319 (1995)
125. A. Haasz, S. Chiu, P. Franzen: *J. Nucl. Mater.* **220–222**, 815 (1995)
126. S. Chiu, A.A. Haasz: *J. Nucl. Mater.* **196–198**, 972 (1992)
127. S. Chiu, A.A. Haasz: *J. Nucl. Mater.* **208**, 282 (1994)
128. S. Chiu, A.A. Haasz: *J. Nucl. Mater.* **210**, 34 (1994)
129. A.A. Haasz, A.Y.K. Chen, J.W. Davis, E. Vietzke: *J. Nucl. Mater.* **248**, 19 (1997)
130. A.Y.K. Chen, J.W. Davis, A.A. Haasz: *J. Nucl. Mater.* **266–269**, 399 (1999)
131. A.Y.K. Chen, J.W. Davis, A.A. Haasz: *J. Nucl. Mater.* **290–293**, 61 (2002)
132. A.Y.K. Chen, J.W. Davis, A.A. Haasz: *J. Nucl. Mater.* **312**, 16 (2003)
133. A.Y.K. Chen, A.A. Haasz, J.W. Davis: *J. Appl. Phys.* **94**, 1617 (2003)
134. R.G. Macaulay-Newcombe, A.A. Haasz, C.H. Wu, J.W. Davis: *J. Nucl. Mater.* **327**, 114 (2004)
135. A. von Keudell, T. Schwarz-Selinger, W. Jacob: *J. Appl. Phys.* **89**, 2979 (2001)
136. A. von Keudell: *Thin Solid Films* **402**, 1 (2002)
137. A. von Keudell, W. Jacob: *Prog. Surf. Sci.* **76**, 21 (2004)
138. M. Meier, A. von Keudell: *J. Appl. Phys.* **90**, 3585 (2001)
139. M. Meier, A. von Keudell: *J. Chem. Phys.* **116**, 5125 (2002)
140. C. Hopf, A. von Keudell, W. Jacob: *J. Appl. Phys.* **93**, 3352 (2003)
141. C. Hopf, A. von Keudell, W. Jacob: *J. Appl. Phys.* **94**, 2373 (2003)
142. C. Hopf, W. Jacob, A. von Keudell: *J. Appl. Phys.* **97**, 094904–1 (2005)
143. W. Jacob, C. Hopf, A. von Keudell, M. Meier, T. Schwarz-Selinger: *Rev. Sci. Instrum.* **74**, 5123 (2003)
144. T. Schwarz-Selinger, A. von Keudell, W. Jacob: *J. Vac. Sci. Technol. A* **18**, 995 (2000)
145. T. Schwarz-Selinger, V. Dose, W. Jacob, A. von Keudell: *J. Vac. Sci. Technol. A* **19**, 101 (2001)
146. C.S. Pitcher, O. Auciello, A.A. Haasz, P.C. Stangeby: *J. Nucl. Mater.* **128–129**, 597 (1984)
147. A.A. Haasz, O. Auciello, P.C. Stangeby: *J. Vac. Sci. Technol. A* **4**, 1179 (1986)
148. E. Vietzke, K. Flaskamp, V. Philipps, G. Esser, P. Wienhold, J. Winter: *J. Nucl. Mater.* **145–147**, 443 (1987)
149. A. Schenk, J. Biener, B. Winter, C. Lutterloh, U. Schubert, J. Küppers: *Appl. Phys. Lett.* **61**, 2414 (1992)
150. J. Biener, U. Schubert, A. Schenk, B. Winter, C. Lutterloh, J. Küppers: *Advan. Mater.* **5**, 639 (1993)
151. J. Biener, U. Schubert, A. Schenk, B. Winter, C. Lutterloh, J. Küppers: *J. Chem. Phys.* **99**, 3125 (1993)
152. J. Biener, A. Schenk, B. Winter, J. Küppers: *J. Electr. Spectr. Rel. Phen.* **64/65**, 331 (1993)
153. J. Biener, A. Schenk, B. Winter, U. Schubert, C. Lutterloh, J. Küppers: *Phys. Rev. B* **49**, 17307 (1994)
154. J. Biener, A. Schenk, B. Winter, C. Lutterloh, U. Schubert, J. Küppers: *Surf. Sci.* **307–309**, 228 (1994)
155. A. Horn, A. Schenk, J. Biener, B. Winter, C. Lutterloh, M. Wittmann, J. Küppers: *Chem. Phys. Lett.* **231**, 193 (1994)
156. A. Schenk, B. Winter, J. Biener, C. Lutterloh, U. Schubert, J. Küppers: *J. Appl. Phys.* **77**, 2462 (1995)
157. J. Küppers: *Surf. Sci. Rep.* **22**, 249 (1995)

158. M. Wittmann, J. Küppers: *J. Nucl. Mater.* **227**, 186 (1996)
159. J. Roth, C. García-Rosales: *Nucl. Fusion* **36**, 1647 (1996). See also corrigendum: J. Roth, C. García-Rosales, *Nucl. Fusion* **37**, 897 (1997).
160. V. Philipps, K. Flaskamp, E. Vietzke: *J. Nucl. Mater.* **122–123**, 1440 (1984)
161. J.W. Davis, A.A. Haasz, P.C. Stangeby: *J. Nucl. Mater.* **155–157**, 234 (1988)
162. E. Vietzke, V. Philipps, K. Flaskamp, P. Koidl, C. Wild: *Surf. Coat. Technol.* **47**, 156 (1991)
163. O. Auciello, A.A. Haasz, P.C. Stangeby: *Radiat. Eff.* **89**, 63 (1985)
164. J. Roth, E. Vietzke, A.A. Haasz: In: *Atomic and Plasma-Material Interaction Data for Fusion* Suppl. *Nucl. Fusion* **1**, 63 (1991)
165. C.M. Braganza, S.K. Erents, G.M. McCracken: *J. Nucl. Mater.* **75**, 209 (1978)
166. R. Yamada, K. Nakamura, K. Sone, M. Saidoh: *J. Nucl. Mater.* **95**, 278 (1980)
167. E. Vietzke, V. Philipps: *Nucl. Instrum. Meth. B* **23**, 449 (1987)
168. J.W. Davis, A.A. Haasz: *J. Nucl. Mater.* **149**, 349 (1987)
169. A.A. Haasz, J.W. Davis: *J. Nucl. Mater.* **175**, 84 (1990)
170. J.W. Davis, A.A. Haasz, P.C. Stangeby: *J. Nucl. Mater.* **145–147**, 417 (1987)
171. R. Yamada, K. Sone: *J. Nucl. Mater.* **116**, 200 (1983)
172. R. Yamada: *J. Nucl. Mater.* **145–147**, 359 (1987)
173. J. Roth, J. Bohdanský: *Nucl. Instrum. Meth. B* **23**, 549 (1987)
174. A.A. Haasz, B.V. Mech, J.D. Davis: *J. Nucl. Mater.* **231**, 170 (1996)
175. B.V. Mech, A.A. Haasz, J.W. Davis: *J. Nucl. Mater.* **241–243**, 1147 (1997)
176. B.V. Mech, A.A. Haasz, J.W. Davis: *J. Nucl. Mater.* **255**, 153 (1998)
177. L.I. Vergara, F.W. Meyer, H.F. Krause: *J. Nucl. Mater.* **347**, 118 (2005)
178. F.W. Meyer, H.F. Krause, L.I. Vergara: *J. Nucl. Mater.* **337–339**, 922 (2005)
179. F.W. Meyer, L.I. Vergara, H.F. Krause: *Phys. Scripta* **T124**, 44 (2006)
180. L.I. Vergara, F.W. Meyer, H.F. Krause, P. Träskelin, K. Nordlund, E. Salonen: *J. Nucl. Mater.* **357**, 9 (2006)
181. M. Küstner, W. Eckstein, V. Dose, J. Roth: *Nucl. Instrum. Meth. B* **145**, 320 (1998)
182. M. Balden, E. de Juan Pardo, I. Quintana, B. Ciecwi, J. Roth: *J. Nucl. Mater.* **337–339**, 980 (2005)
183. E. Vietzke, V. Philipps: *Fusion Technol.* **15**, 108 (1989)
184. B.M.U. Scherzer, R. Behrisch, W. Eckstein, U. Littmark, J. Roth, M.K. Sinha: *J. Nucl. Mater.* **63**, 100 (1976)
185. G. Staudenmaier, J. Roth, R. Behrisch, J. Bohdanský, W. Eckstein, P. Staib, S. Matteson, S.K. Erents: *J. Nucl. Mater.* **84**, 149 (1979)
186. J. Roth, B.M.U. Scherzer, R.S. Blewer, D.K. Brice, S.T. Picraux, W.R. Wampler: *J. Nucl. Mater.* **93–94**, 601 (1980)
187. W.R. Wampler, D.K. Brice, C.W. Magee: *J. Nucl. Mater.* **102**, 304 (1981)
188. B.M.U. Scherzer, R.A. Langley, W. Möller, J. Roth, R. Schulz: *Nucl. Instrum. Meth.* **194**, 497 (1982)
189. M. Braun, B. Emmoth: *J. Nucl. Mater.* **128–129**, 657 (1984)
190. W. Möller, B.M.U. Scherzer: *Appl. Phys. Lett.* **50**, 1870 (1987)
191. B.M.U. Scherzer, M. Wielunski, W. Möller, A. Turos, J. Roth: *Nucl. Instrum. Meth. B* **33**, 714 (1988)
192. W. Möller, B.M.U. Scherzer: *J. Appl. Phys.* **64**, 4860 (1988)
193. W. Möller: *J. Nucl. Mater.* **162–164**, 138 (1989)
194. B.L. Doyle, P.S. Percy: *Appl. Phys. Lett.* **34**, 811 (1979)
195. J. Roth, J. Bohdanský: *Appl. Phys. Lett.* **51**, 964 (1987)

196. J. Roth, R.A. Zuhr, S.P. Withrow, W.P. Eatherly: *J. Appl. Phys.* **63**, 2603 (1988)
197. K. Niwase, M. Sugimoto, T. Tanabe, F.E. Fujita: *J. Nucl. Mater.* **155–157**, 303 (1988)
198. R. Siegele, J. Roth, B.M.U. Scherzer, S.J. Pennycook: *J. Appl. Phys.* **73**, 2225 (1993)
199. T. Schwarz-Selinger, A. von Keudell, W. Jacob: *J. Appl. Phys.* **86**, 3988 (1999)
200. J. Winter, H.G. Esser, P. Wienhold, V. Philipps, E. Vietzke, K.H. Besocke, W. Möller, B. Emmoth: *Nucl. Instrum. Meth. B* **23**, 538 (1987)
201. B. Lersmacher, H. Lydtin, W.F. Knippenberg, A.W. Moore: *Carbon* **5**, 205 (1967)
202. J. Roth: In *Atomic and Plasma-Material Interaction Processes in Controlled Thermonuclear Fusion*, ed. by R.K. Janev, H.W. Drawin, (Elsevier, Amsterdam 1993), pp. 381
203. C.S. Pitcher, G.M. McCracken, D.H.J. Goodall, A.A. Haasz, G.F. Matthews, P.C. Stangeby: *Nucl. Fusion* **26**, 1641 (1986)
204. P. Kornejew, W. Bohmeyer, H.D. Reiner: *Phys. Scripta* **T81**, 40 (1990)
205. R. Ruggiéri, E. Gauthier, J. Hogan, J.M. Layet, T. Loarer: *J. Nucl. Mater.* **266–269**, 660 (1999)
206. A. Cambe, E. Gauthier, J. Hogan, J.M. Layet: *J. Nucl. Mater.* **313–316**, 364 (2003)
207. A. Pospieszczyk, V. Philipps, A. Huber, A. Kirschner, B. Schweer, E. Vietzke: *Phys. Scripta* **T81**, 48 (1999)
208. A. Kallenbach, A. Bard, D. Coster, R. Dux, C. Fuchs, J. Gafert, A. Herrmann, R. Schneider, ASDEX Upgrade Team: *J. Nucl. Mater.* **266–269**, 343 (1999)
209. T. Nakano, H. Kubo, S. Higashijima, N. Asakura, H. Takenaga, T. Sugie, K. Itami: *Nucl. Fusion* **42**, 689 (2002)
210. J. Roth, R. Preuss, W. Bohmeyer, S. Brezinsek, A. Cambe, E. Casarotto, R. Doerner, E. Gauthier, G. Federici, S. Higashijima, J. Hogan, A. Kallenbach, A. Kirschner, H. Kubo, J. Layet, T. Nakano, V. Philipps, A. Pospieszczyk, R. Pugno, R. Ruggieri, B. Schweer, G. Sergienko, M. Stamp: *Nucl. Fusion* **44**, L21 (2004)
211. V. Dose, R. Preuss, J. Roth: *J. Nucl. Mater.* **288**, 153 (2001)
212. V. Dose: *Rep. Prog. Phys.* **66**, 1421 (2003)
213. R. Yamada: *J. Vac. Sci. Technol. A* **5**, 305 (1987)
214. R. Yamada: *J. Nucl. Mater.* **174**, 118 (1990)
215. A.A. Haasz, O. Auciello, P.C. Stangeby, I.S. Youle: *J. Nucl. Mater.* **128–129**, 593 (1984)
216. A.A. Haasz, J.W. Davis, O. Auciello, P. Stangeby, E. Vietzke, K. Flaskamp, V. Philipps: *J. Nucl. Mater.* **145–147**, 412 (1987)
217. C. Hopf, A. von Keudell, W. Jacob: *Nucl. Fusion* **42**, L27 (2002)
218. W. Jacob, C. Hopf, M. Meier, T. Schwarz-Selinger: In *Nuclear Fusion Research – Understanding Plasma–Surface Interaction*, 1st edn., Springer Series in Chemical Physics (Springer, Berlin 2005), pp. 249
219. W. Jacob, C. Hopf, M. Schlüter: *Phys. Scripta* **T124**, 32 (2006)
220. W. Eckstein: *Computer Simulation of Ion Solid Interactions*, Springer Series in Materials Science, Vol. 10, (Springer, Berlin, Heidelberg 1991), Russ. translation: (MIR, Moscow 1995)
221. J. Roth, J. Bohdanský, J.B. Roberto: *J. Nucl. Mater.* **128–129**, 534 (1984)

222. J. Roth, C. García-Rosales, R. Behrisch, W. Eckstein: *J. Nucl. Mater.* **191**, 45 (1992)
223. R. Schwörer, H. Plank, J. Roth: *J. Nucl. Mater.* **241–243**, 1156 (1997)
224. V.K. Alimov, R. Schwörer, B.M.U. Scherzer, J. Roth: *J. Nucl. Mater.* **187**, 191 (1992)
225. R. Schwörer, J. Roth: *J. Appl. Phys.* **77**, 3812 (1995)
226. C. García-Rosales, J. Roth: *J. Nucl. Mater.* **196–198**, 573 (1992)
227. C. García-Rosales, J. Roth, R. Behrisch: *J. Nucl. Mater.* **212–215**, 1211 (1994)
228. M. Balden, C. García-Rosales, R. Behrisch, J. Roth, P. Paz, J. Etxeberria: *J. Nucl. Mater.* **290–293**, 52 (2001)
229. Y. Yao, Z. Hargitai, M. Albert, R.G. Albridge, A.V. Barnes, J.M. Gilligan, B.P. Ferguson, G. Lüpke, V.D. Gordon, N.H. Tolk, J.C. Tully, G. Betz, W. Husinsky: *Phys. Rev. Lett.* **81**, 550 (1998)
230. R.K. Gould: *J. Chem. Phys.* **63**, 1825 (1975)
231. M. Balden, J. Roth, E. de Juan Pardo, A. Wiltner: *J. Nucl. Mater.* **313–316**, 348 (2003)
232. T. Zecho, A. Güttler, X. Sha, B. Jackson, J. Küppers: *J. Chem. Phys.* **117**, 8486 (2002)
233. B.V. Mech, A.A. Haasz, J.W. Davis: *J. Appl. Phys.* **84**, 1655 (1998)
234. J. Bohdansky, J. Roth, H. Bay: *J. Appl. Phys.* **51**, 2861 (1980)
235. J. Roth: *Phys. Scripta* **T124**, 37 (2005)
236. C. Hopf, W. Jacob: *J. Nucl. Mater.* **342**, 141 (2005)
237. E. Ghio, L. Mattera, C. Salvo, F. Tommasini, U. Valbusa: *J. Chem. Phys.* **73**, 556 (1980)
238. J. Pillath, J. Winter, F. Waelbroek: In *Amorphous hydrogenated carbon films*, ed. by P. Koidl, P. Oelhafen (Les Éditions de Physique, Les Ulis, 1987), p. 449
239. E. Salonen, K. Nordlund, J. Tarus, T. Ahlgren, J. Keinonen, C. Wu: *Phys. Rev. B* **60**, R14005–1–4 (1999)
240. E. Salonen, K. Nordlund, J. Keinonen, N. Runeberg, C. Wu: *J. Appl. Phys.* **92**, 2216 (2002)
241. E. Salonen, K. Nordlund, J. Keinonen, C. Wu: *Contrib. Plasma Phys.* **42**, 458 (2002)
242. E. Salonen, K. Nordlund, J. Keinonen, C. Wu: *J. Nucl. Mater.* **313–316**, 404 (2003)
243. P. Träskelin, K. Nordlund, J. Keinonen: *Nucl. Instrum. Meth. B* **228**, 319 (2005)
244. K. Nordlund: *Phys. Scripta* **T124**, 53 (2006)
245. S.J. Stuart, P.S. Krstić, T.A. Embry, C.O. Reinhold: *Nucl. Instrum. Meth. B* **255**, 202 (2007)
246. P.S. Krstić, C.O. Reinhold, S.J. Stuart: *Europhys. Lett.* **77**, 33002 (2007)
247. P.S. Krstić, S.J. Stuart, C.O. Reinhold: *AIP Conference Proceedings* **876**, 201 (2006)
248. C.O. Reinhold, P.S. Krstić, S.J. Stuart: *Nucl. Instrum. Meth. B* **258**, 274 (2007)
249. R.G. Macaulay-Newcombe, A.A. Haasz, J.W. Davis: *J. Nucl. Mater.* **337–339**, 857 (2005)
250. A.A. Haasz, J.W. Davis: *Fus. Sci. Technol.* **50**, 58 (2006)

251. P. Franzen: Report IPP 9/92, Garching (1993)
252. K. Maruyama, W. Jacob, J. Roth: *J. Nucl. Mater.* **264**, 56 (1999)
253. W.M. Wang, J. Roth, W. Eckstein, R. Schwoerer, H. Plank, M. Du: *Nucl. Instrum. Meth. B* **129**, 210 (1997)
254. M. Balden, K.U. Klages, W. Jacob, J. Roth: *J. Nucl. Mater.* **341**, 31 (2005)
255. C. Li, T.C. Brown: *Carbon* **39**, 725 (2001)
256. J.O. Müller, D.S. Su, R.E. Jentoft, J. Kröhnert, F.C. Jentoft, R. Schlögl: *Catalysis Today* **102–103**, 259 (2005)
257. H. Marsh, K. Kuo: In *Introduction to Carbon Science*, ed. by H. Marsh, (Butterworths, London 1989), p. 107
258. B.R. Stanmore, J.F. Brilhac, P. Gilot: *Carbon* **39**, 2247 (2001)
259. J.W. Davis, C.G. Hamilton, A.A. Haasz: *J. Nucl. Mater.* **288**, 148 (2001)
260. D.E. Rosner, H.D. Allendorf: *Kinetics of the attack of refractory materials by dissociated gases* (Plenum, New York 1970), and references therein
261. E. Vietzke, T. Tanabe, V. Philipps, M. Erdweg, K. Flaskamp: *J. Nucl. Mater.* **145–147**, 425 (1987)
262. A. Refke, V. Philipps, E. Vietzke: *J. Nucl. Mater.* **250**, 13 (1997)
263. E. Vietzke, A.A. Haasz: In *Physical Processes of the Interaction of Fusion Plasmas with Solids*, ed. by W.O. Hofer, J. Roth (Academic, New York 1996), pp. 135
264. E. Hechtel, J. Bohdansky: *J. Nucl. Mater* **141–143**, 139 (1986)
265. E. Hechtel, J. Bohdansky: *J. Nucl. Mater* **154**, 201 (1988)
266. C. Hopf, M. Schlüter, W. Jacob: to be submitted to *J. Appl. Phys.* (2007)
267. C. Hopf, M. Schlüter, W. Jacob: *Appl. Phys. Lett.* **90**, in print (2007)
268. B. Landkammer, A. von Keudell, W. Jacob: *J. Nucl. Mater.* **264**, 48 (1999)
269. G. Adamopoulos, C. Godet, B. Drévillon, Y. Sato, D.N. Batchelder, A. Grosman, C. Ortega: *Diamond Relat. Mater.* **12**, 983 (2003)
270. A.M. Baranov, V.V. Sleptsov, A.A. Nefedov, A.E. Varfolomeev, L. Calliari: *Diamond Relat. Mater.* **13**, 1356 (2004)
271. K.K. Hirakuri, K. Kuwashima, K. Tatsuta, K. Sato: *Diamond Relat. Mater.* **14**, 1067 (2005)
272. W.L. Hsu: *J. Vac. Sci. Technol A* **7**, 1047 (1989)
273. D. Mueller, W. Blanchard, J. Collins, J. Hosea, J. Kamperschroer, P.H. LaMarche, A. Nagy, D.K. Owens, C.H. Skinner: *J. Nucl. Mater.* **241–243**, 897 (1997)
274. W. Jacob, B. Landkammer, C. Wu: *J. Nucl. Mater.* **266–269**, 552 (1999)
275. J.S. Hu, J.G. Li, X.M. Wang, the HT-7 team: *Plasma Phys. Control. Fusion* **47**, 1271 (2005)
276. J.S. Hu, J.G. Li, X.M. Wang: *J. Nucl. Mater.* **350**, 9 (2006)
277. C. Hopf, V. Rohde, W. Jacob, A. Herrmann, R. Neu, J. Roth, ASDEX Upgrade Team: *J. Nucl. Mater.* **363–365**, 882 (2007)
278. S. Fujimura, K. Shinagawa, M.T. Suzuki, M. Nakamura: *J. Vac. Sci. Technol. B* **9**, 357 (1991)
279. T.E.F.M. Standaert, P.J. Matsuo, X. Li, G.S. Oehrlein, T.M. Lu, R. Gutmann, C.T. Rosenmayer, J.W. Bartz, J.G. Langan, W.R. Entley: *J. Vac. Sci. Technol. A* **19**, 435 (2001)
280. W. Jacob, C. Hopf, M. Schlüter: *Appl. Phys. Lett.* **86**, 204103 (2005)
281. S. Grigull, W. Jacob, D. Henke, C. Spaeth, L. Sümmchen, W. Sigle: *J. Appl. Phys.* **83**, 5185 (1998)

282. S. Grigull, R. Behrisch, S. Parascandola: *J. Nucl. Mater.* **275**, 158 (1999)
283. P. Hammer, W. Gissler: *Diamond Relat. Mater.* **5**, 1152 (1996)
284. M. Schlüter, C. Hopf, T. Schwarz-Selinger, W. Jacob: to be submitted to *J. Appl. Phys.* (2007)
285. K.J. Clay, S.P. Speakman, G.A.J. Amaratunga, S.R.P. Silva: *J. Appl. Phys.* **79**, 7227 (1996)
286. C. Spaeth, U. Kreissig, F. Richter: *Thin Solid Films* **355–356**, 64 (1999)
287. S.E. Rodil, N.A. Morrison, J. Robertson, W.I. Milne: *Phys. Stat. Sol. (A)* **174**, 25 (1999)
288. J. Hong, G. Turban: *Diamond Relat. Mater.* **8**, 572 (1999)
289. J. Hong, A. Granier, A. Goulet, G. Turban: *Diamond Relat. Mater.* **9**, 573 (2000)
290. N. Hellgren, M.P. Johansson, B. Hjörvarsson, E. Broitman, M. Östblom, B. Liedberg, L. Hultman, J.E. Sundgren: *J. Vac. Sci. Technol. A* **18**, 2349 (2000)
291. N. Hellgren, M.P. Johansson, E. Broitman, P. Sandström, L. Hultman, J.E. Sundgren: *Thin Solid Films* **382**, 146 (2001)
292. N.A. Morrison, S.E. Rodil, J. Robertson, W.I. Milne: *J. Appl. Phys.* **89**, 5754 (2001)
293. T. Schwarz-Selinger, C. Hopf, C. Sun, W. Jacob: *J. Nucl. Mater.* **363–365**, 174 (2007)
294. J.W. Butterbaugh, D.C. Gray, H.H. Sawin: *J. Vac. Sci. Technol. B* **9**, 1461 (1991)
295. G.S. Oehrlein, D. Zhang, D. Vender, M. Haverlag: *J. Vac. Sci. Technol. A* **12**, 323 (1994)
296. G.S. Oehrlein, D. Zhang, D. Vender, O. Joubert: *J. Vac. Sci. Technol. A* **12**, 333 (1994)
297. T.E.F.M. Standaert, M. Schaepkens, P.G.M. Sebel, N.R. Rueger, G.S. Oehrlein: *J. Vac. Sci. Technol. A* **16**, 239 (1998)
298. T. Standaert, C. Hedlund, E.A. Joseph, G.S. Oehrlein, T.J. Dalton: *J. Vac. Sci. Technol. A* **22**, 53 (2004)
299. D. Humbird, D.B. Graves, X.F. Hua, G.S. Oehrlein: *Appl. Phys. Lett.* **84**, 1073 (2004)

Index

- activation energy
 - desorption, 53
 - Gaussian distribution, 18
 - hydrocarbon release, 37
 - hydrogen desorption, 37
- amorphisation, 26
- annealing, 33
- Bayesian theory, 8, 29
- bond breaking, 47, 48, 53, 60
- cascade mixing, 3
- catalyst, 57
- cavity probe, 12
- chemical erosion, 4, 14
 - released species, 18, 20
- chemical sputtering, 5, 12, 14
 - combined irradiation, 20, 32, 60
 - doping, 37
 - energy dependence, 22
 - flux dependence, 27, 28
 - model, 47
 - modelling, 41
 - molecular ion, 38
 - reactive species, 57
 - released species, 29
 - temperature dependence, 21
- damage formation, 25
- decomposition
 - hydrocarbon, 42
- desorption, 15, 48, 53, 58
- diffusion, 42, 50, 55
- dissociation
 - hydrocarbon, 11
 - molecule, 11
- electron high energy loss spectroscopy(HREELS), 14
- ellipsometry, 6, 10, 11, 14, 34
- etching
 - dry, 3
 - ion-assisted, 4
 - plasma, 3
 - reactive ion, 4
 - wet, 3
- excitation
 - electronic, 33
- flux dependence, 29
- graphitization, 20, 27
- hybridisation, 14, 16
- hydrogenation, 15, 16
- implantation range, 27
- interaction potential
 - hydrocarbon (Brenner), 52
- ionization, 11
- isotope effect, 25, 48, 54
- isotope exchange, 19
- isotope sputtering, 53
- mass spectrometer
 - background signal, 9
 - line-of-sight, 8
 - quadrupole, 10
 - remote, 7, 19
 - sensitivity, 8
 - time-of-flight, 12
- mass spectrometry, 6, 8, 33, 46, 61
 - molecular beam (MBMS), 9, 12, 34
- molecular dynamics, 50
- molecule
 - formation, 2, 5, 15
 - hydrocarbon, 11

- optical emission spectroscopy, 11, 61
- production rate
 - methane, 33
- production yield
 - C₂, 30
 - hydrocarbon, 34
 - methane, 23, 33
- radiation damage, 26, 27, 42, 53, 55
- radiation-enhanced sublimation (RES), 5
- radical
 - hydrocarbon, 8, 11
 - methyl, 14
 - species, 33
 - suprathemal, 6
 - volatile, 1
- range, 49, 55
- reaction rate, 57
- reaction yield, 57
- recoil implantation, 3
- selfsputtering, 5
- simultaneous bombardment, 13, 61
- sputtering of
 - carbides, 3
 - nitrides, 3
 - oxides, 3
- sticking
 - probability, 7, 12
- sublimation temperature, 5
- surface
 - altered layer, 3
 - roughness, 11
- surface binding energy, 3, 5, 48
- surface topography, 38
- swift chemical sputtering, 6
- synergistic effect, 33
- target
 - a-C:H layer, 60
 - hard, 19, 27
 - soft, 19
 - graphite
 - grade, 17, 25
 - pre-irradiated, 46
 - type, 25
 - metal-doped carbon, 8
 - pyrolytic graphite, 14
- thermal desorption, 3, 6
- thermal desorption spectroscopy (TDS), 14
- threshold energy, 4, 5, 25, 53, 54
- weight loss, 7